Author's Version

Aluminum diffusion inhibiting properties of Ti_5Si_3 at 900 °C and its beneficial properties on Al-rich oxidation protective coatings on γ-TiAl

Peter-Philipp Bauer[a], Radosław Swadźba[b], Lisa Klamann[a], Nadine Laska[a]

[a]German Aerospace Center (DLR), Institute of Materials Research, Linder Hoehe, D-51147 Cologne, Germany,

[b]Łukasiewicz Research Network - Institute for Ferrous Metallurgy, Gliwice, Poland

Corrosion Science (2022)

https://doi.org/10.1016/j.corsci.2022.110265

Aluminum diffusion inhibiting properties of Ti_5Si_3 at 900 °C and its beneficial properties on Al-rich oxidation protective coatings on γ-TiAl

Peter-Philipp Bauer[a], Radosław Swadźba[b], Lisa Klamann[a], Nadine Laska[a]

[a]*German Aerospace Center (DLR), Institute of Materials Research, Linder Hoehe, D-51147 Cologne, Germany,*
[b]*Łukasiewicz Research Network - Institute for Ferrous Metallurgy, Gliwice, Poland*

*corresponding author. E-mail address: peter-philipp.bauer@dlr.de

The goal of the paper was to elucidate the effect of a Ti_5Si_3 interlayer on the high temperature oxidation resistance of the Al-Ti coatings. During cyclic oxidation at 900 °C for 1000 1 h cycles, the coating system with a Ti_5Si_3 interlayer maintained the Al-rich phases of $TiAl_3$ and $TiAl_2$ in the Al-Ti top layer around 5-10 times longer compared to a coating without intermediate barrier layer. Moreover, the substrate alloying elements (Nb and Cr) are suggested to have a noticeably positive impact on the reduced Al diffusion due to segregations at the grain boundaries in the Ti_5Si_3 interlayer.

Keywords: Ti_5Si_3 interlayer, Al diffusion, diffusion barrier, γ-TiAl alloys, oxidation protective Al-Ti coating, mass gain analysis, magnetron sputtering

1. Introduction

Surface modifications are a feasible way to improve the oxidation resistance of γ-titanium aluminide (TiAl) alloys [1, 2]. So far, the service temperature of TiAl alloys is limited to temperatures below 800 °C [3-5]. At higher temperatures, TiAl suffers

from the formation of titanium oxides and nitrides, promoting high oxidation rates and thus accelerating the failure of the component [3, 5-8]. To overcome this issue, the formation of the fast-growing oxide of TiO_2 needs to be inhibited and a dense and slow growing oxide need to be formed instead, such as Al_2O_3 [9]. This can be achieved by enrichment of the TiAl surface with Al [10] by, for instance, pack cementation processes [11, 12] or overlaying coatings [13-15], that provide a good oxidation protection to some extent. At longer oxidation times or higher temperatures these coatings suffer from the depletion of Al due the formation of alumina as well as the inward diffusion of Al into the substrate material [11, 13, 16]. Eventually, this leads to the formation of non-protective oxides and nitrides. However, the addition of silicon to Al-rich coatings shows an improvement in the oxidation resistance and provides a decent protection for a longer time and/or at higher temperatures [17-31]. An overview of the different Si containing coatings for TiAl as well as the development of various TiAl-Si alloys is given by the recent review [32].

In the Al-Si based coatings, one of the preferentially formed silicides is Ti_5Si_3. Since Ti_5Si_3 provides a homogeneity range [33], it could act as a Ti getter and reduce its activity [20]. During the oxidation of the Al-rich $TiAl_2$ and $TiAl_3$ phases, Ti_5Si_3 could therefore counteract the depletion of these phases by gettering the “released” Ti [21] or hinder the outwards diffusion of Ti from the TiAl substrate to the coating [20]. In addition, the formed Ti_5Si_3 phase, often located at the grain boundaries, could serve as a diffusion barrier for Al and therefore inhibit the diffusion of Al from the coating into the substrate [21].

At temperatures below 600 °C, the properties of Ti_5Si_3 as a diffusion barrier for pure Al on a Si substrates were already investigated [34]. However, at higher temperatures no systematical studies were published so far. Therefore, the present work

addresses this question by investigating the properties of the Ti_5Si_3 phase as a diffusion barrier for Al at 900 °C on titanium aluminide alloys. Therefore, magnetron sputtering was used to deposit a Ti_5Si_3 interlayer on different γ-TiAl substrates followed by the deposition of an 70Al-30Ti (in at.%) top layer. For comparison, an Al-Ti layer was deposited without the Ti_5Si_3 interlayer. These coating systems were studied by cyclic oxidation tests at 900° C. The results obtained within this study provide insight into the suitability as oxidation protection of these coating system on TiAl for future long-term applications or at higher service temperatures.

2. Methods

Two different γ-TiAl alloys were used as substrate materials: The Nb containing TNB-V2 alloy (Ti: 46,8 at.%, Al: 45 at.%, Nb: 8 at.%, C: 0.2 at.%) and the Nb and Cr containing TiAl48-2-2 alloy (Ti: 48 at%, Al: 48 at.%, Nb: 2 at.%, Cr: 2 at.%). The material was supplied by GFE – GESELLSCHAFT FÜR ELEKTROMETALLURGIE. Flat coin samples with a diameter of 15 mm with a 2 mm borehole for hanging were produced by electrical discharge machining (EDM). The thicknesses of the samples varied from 1 mm for the TNB-V2 substrate and 2 mm for the TiAl48-2-2 substrate. Vibratory finishing was used for surface finishing of the TNB-V2 substrates. The TiAl48-2-2 alloy was grinded with SiC emery paper with a grit of 800. All specimens had a roughness below Sa = 1.6 µm and were cleaned ultrasonically in ethanol prior the coating deposition process.

An industrial size IMPAX 100 HT system from *SVS VACUUM COATING TECHNOLOGY* was utilized for the coating deposition by DC magnetron sputtering. The sputter processes, starting with Argon plasma etching, took place under vacuum with an argon flow of 300 sccm resulting in a pressure of 5.1×10^{-3} mbar. The elemental target materials of Ti, Al, and Si with purity of >99,99% were supplied by EVOCHEM. The

deposition of the dual layer coating system was applied in a one-batch process. Therefore, the samples were rotated in a two-fold rotation between the Ti and the Si target for 75 minutes. Afterwards, the sputtering sources were turned off and the samples were turned between the Ti and Al targets without venting of the sputter chamber. The deposition time of the Al-Ti top layer was 4 h. As reference the single layer coating of Al-Ti without Ti_5Si_3 interlayer was deposited for 4 h and 24 minutes in order to achieve a similar thickness as the dual layer coating system with the same process conditions.

The coating microstructures in the as-deposited condition were analyzed using a BRUKER D8 ADVANCED diffractometer with a copper X-ray tube in Bragg-Brentano-geometry. Moreover, the phase development during high temperature exposure in laboratory air were examined by high-temperature X-ray diffraction (HT-XRD) using the same system equipped with a high temperature oven chamber HTK 1200N from *ANTON PAAR* for *in situ* investigation. A heating rate of 45 K/min was set for the HT-XRD analysis starting at room temperature up to 900 °C. During the heating one measurement was performed every minute. When 900 °C was reached, every 15 minutes one measurement was performed.

Cyclic oxidation tests were performed in a self-constructed automatic test rig which was calibrated and set to 900°C in laboratory air. One cycle consisted of a 60 min period in the furnace and followed by a 10 min forced air cooling period in order to reach temperatures below 50 °C. The weight gains of the single and dual layer coated samples as well as of the bare TiAl alloys were measured with a ME 5-OCE scale from SARTORIUS. In addition, XRD measurements were conducted after 10, 50, 100, 500 and 1000 cycles using the BRUKER D8 ADVANCED diffractometer.

The microstructural investigations were performed using scanning electron microscopy (SEM) as well as scanning transmission electron microscopy (STEM). A *FEI* Helios NanoLab 600i equipped with UltraDry energy-dispersive X-ray spectroscopy (EDS) from THERMO FISHER SCIENTIFIC was used for SEM investigations as well as for FIB lamella preparation. The high-resolution investigations of the coatings were performed using Scanning Transmission Electron Microscope (STEM) FEI TITAN 80-300 operating at 300 kV with Z-sensitive High Angle Annular Dark Field (HAADF) and Annular Dark Field (ADF) detectors. Both systems allowed a chemical analysis by energy-dispersive X-ray spectroscopy (EDS).

3. Results

3.1. Investigations of the coating microstructure after deposition by magnetron sputtering and during heating-up period and the early stage of isothermal oxidation at 900 °C

Figure 1a presents the cross-sectional SEM image of the dual layer system on the TNB-V2 alloy in the as-deposited state. The dual coating of Al-Ti and Ti-Si, as well as the single deposited Al-Ti layer exhibits an excellent adhesion on the TNB-V2 and on TiAl48-2-2. The dual layer system shows a coating thickness of 11-12 µm in total whereby about 1.2 µm is related to the Ti-Si interlayer. Moreover, the presence of elongated vertical pores in the Al-Ti top coating indicates a columnar growth during the magnetron sputtering deposition process. The 10-11 µm thick Al-Ti top layer of the dual layer system reveals an average chemical composition of 70Al-30Ti (in at.%), measured by EDS, and a two-phase microstructure with a bright and a dark phase. EDS analysis of the Ti-Si interlayer showed a chemical composition of 62Ti-38Si at.%. X-ray diffraction measurement (Figure 1b) revealed the presence of a crystalline microstructure of the Al-Ti top layer consisting of the metastable tetragonal Ti_5Al_{11}

phase (darker color phase in the SEM micrograph) and the tetragonal $TiAl_3$ (brighter color phase in the SEM micrograph) phase. The reflexes of the Ti_5Si_3 phase from the interlayer could not be detected by using Bragg-Brentano geometry due to the coating thickness of the top layer. The $TiAl_3$ reflexes are not clearly distinguishable from the Ti_5Al_{11} reflexes in XRD. Therefore, the formation of the metastable Ti_5Al_{11} as well as the $TiAl_3$ phase were confirmed by TEM. Figure 1c shows a bright field TEM image of the fine-grained microstructure (< 500 nm) of the Al-Ti top layer. The dark field TEM image of the same region is presented in Figure 1d which shows the grains that were analyzed by selected area electron diffraction (SAED) in Figure 1c.

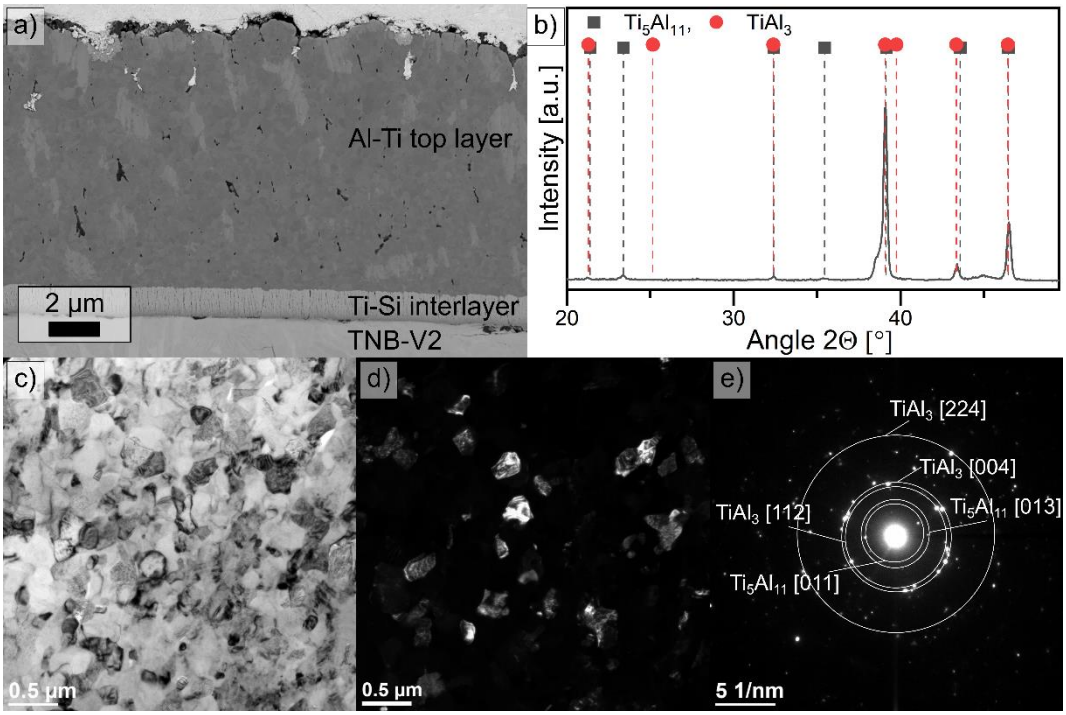

Figure 1: SEM micrograph of the Al-Ti/Ti-Si dual layer coated TNB-V2 alloy (a) with the corresponding diffractogram (b) as well as the TEM images of the Al-Ti top layer in bright field (c) and dark field (d) with the diffraction pattern (e)

The Ti-Si interlayer possesses a columnar morphology (**Figure 2**a). For a more detailed analysis, high resolution TEM investigations were performed. The bright field image in Figure 2b presents a fine microstructure with nanometric grain sizes. Due to the

nanometric grain size the diffraction pattern was created using Fast Fourier Transformation (FFT) of a HRTEM image (Figure 2c). These patterns revealed that besides crystalline areas (I and II) also some amorphous regions (III) were present.

At the coating-substrate interface some oxide particles are visible which are remnants from electrical discharge machining and could not be removed by the vibratory polishing process.

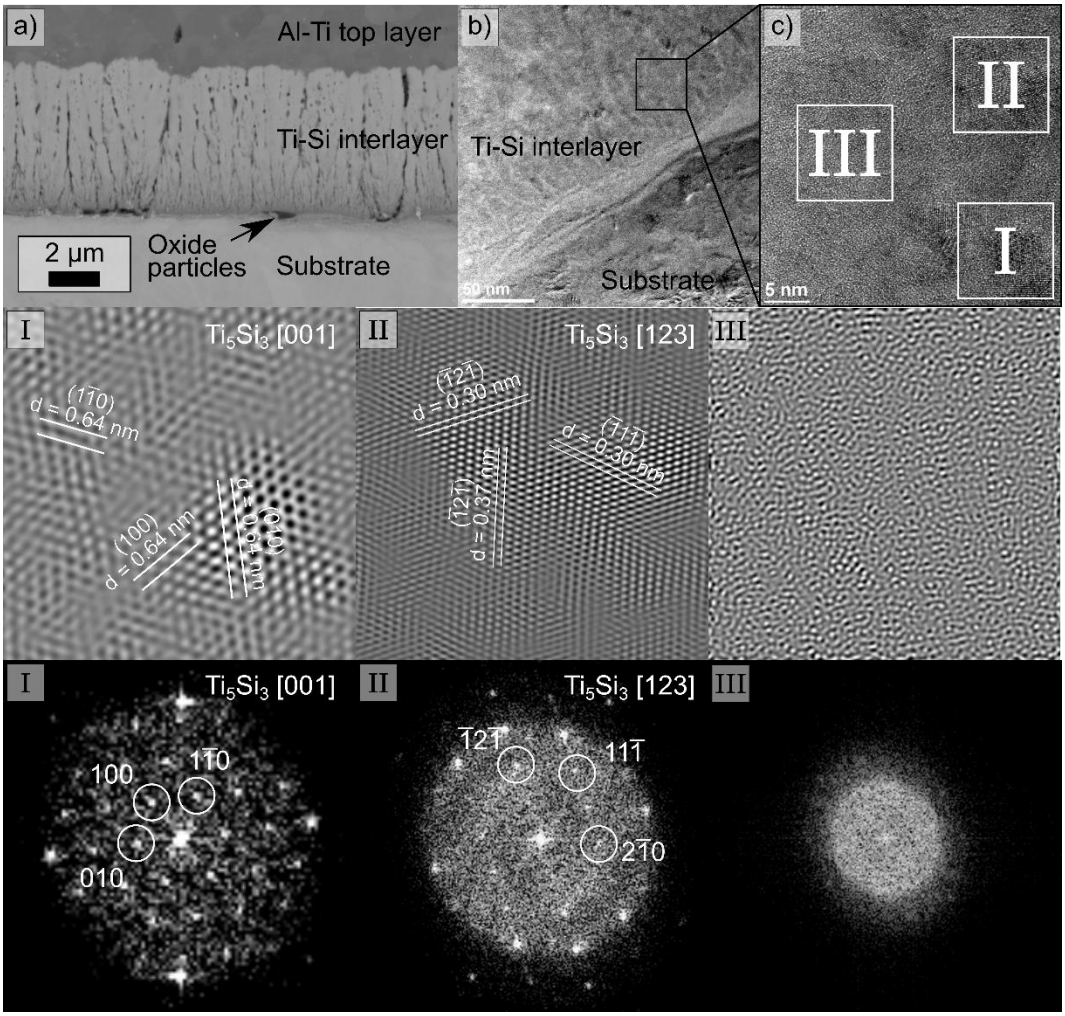

Figure 2: SEM micrograph of the Ti-Si interlayer (a) and HRTEM images of the Ti-Si interlayer (b) with a magnified area (c) and the Inverse Fast Fourier Transformation (IFFT) along with the corresponding diffraction patterns created by Fast Fourier Transformation (I, II, III)

The phase transformations during the heating-up period up to 900°C in laboratory air were analyzed by *in situ* HT-XRD. Sections of the received X-ray diffractograms (from 40° to 48° 2θ in Bragg-Brentano geometry) of each single and

double layer coated TNB-V2 and Ti48-2-2 alloys are presented in **Figure 3**. The transformation of the tetragonal Ti_5Al_{11} and tetragonal $TiAl_3$ phases to the tetragonal $TiAl_2$ phase in the Al-Ti top layer started at around 660 °C as indicated by the appearance of the peak at around 45°. The low temperature polymorph of the tetragonal $TiAl_3$ phase, further referred to as $TiAl_3$ (l), started forming at about 750 °C. This was recognizable due to the peak drifting of the Ti_5Al_{11} phase at 43.2° and 46.3° to higher diffraction angles which is in contrast with the peak shift to lower diffraction angles by the thermal expansion of the lattice. However, in samples with additionally deposited Ti_5Si_3 interlayer a third phase formed in the Al-Ti top layer at even higher temperatures (~775 °C) which was identified as the high temperature polymorph of $TiAl_3$, further referred to as $TiAl_3$ (h).

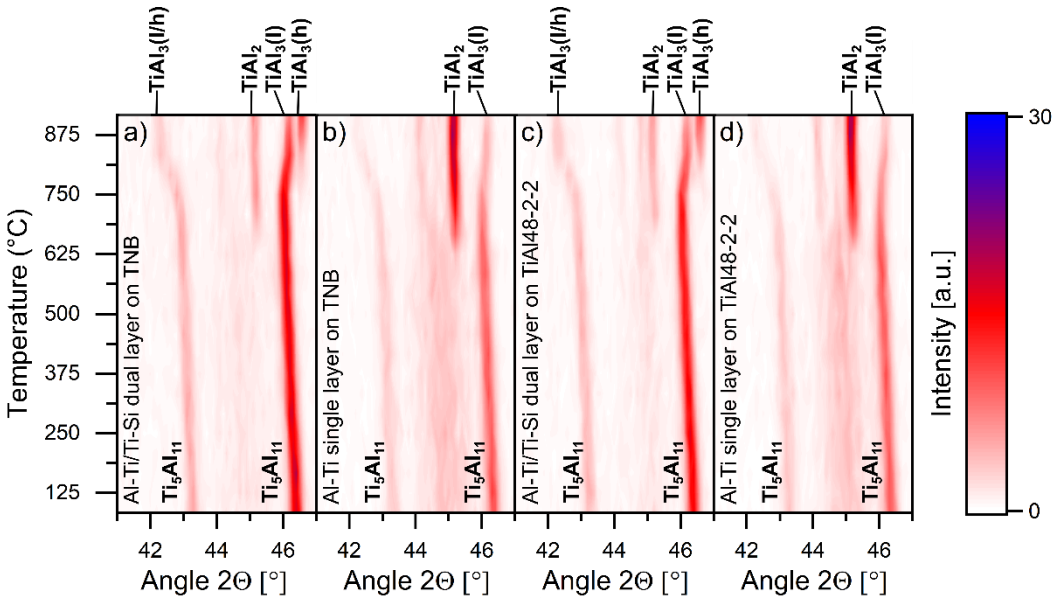

Figure 3: HT-XRD results of the heating process to 900 °C with a heating rate of 45 K/min. The temperature was measured at the beginning of each 1 minute XRD measurement. During the measurement the heating was continiued. a) Ti-Si/Al-Ti dual-layer on TNB-V2 substrate, b) single Al-Ti layer on TNB-V2 substrate, c) Ti-Si/Al-Ti dual-layer on TiAl48-2-2 substrate, d) single Al-Ti layer on TiAl48-2-2 substrate

Figure 4 presents a section of the XRD scans from 21° to 27° 2θ in Bragg-Brentano geometry over a total time of 50 h at 900 °C. Within the first 15 minutes of exposure at the constant temperature of 900 °C, the $TiAl_3$ (l) phase disappeared in both of the Al-Ti single layer coated samples and therefore is not visible in the XRD scans (Figure 4b, d). In contrast, the $TiAl_3$ (h) phase was present for 8.25 h in the Al-Ti top layer of the dual-layer coated TNB-V2 sample (Figure 4a) and 14.85 h for the TiAl48-2-2 sample (Figure 4c). During this time period, no $TiAl_3$ (l) formed indicating a direct transition of the $TiAl_3$ (h) phase to the $TiAl_2$ phase. On the TNB-V2 substrate the $TiAl_3$ (h) phase disappeared faster. In the single layer coated TNB-V2 substrate, the $TiAl_2$ phase transformed to the tetragonal γ-TiAl phase within 35 h. In contrast, the $TiAl_2$ phase is still present after 50 h of oxidation in the samples with additionally deposited Ti-Si interlayer. After 25 h of oxidation, γ-TiAl phase already started to form in the single layered TiAl48-2-2 sample. With regard to the oxidation behavior, all coated samples formed the protective α-Al_2O_3 phase, which is typical for high Al containing TiAl phases, such as $TiAl_2$ and $TiAl_3$. There was no evidence in the HT-XRD measurements for the formation of TiO_2.

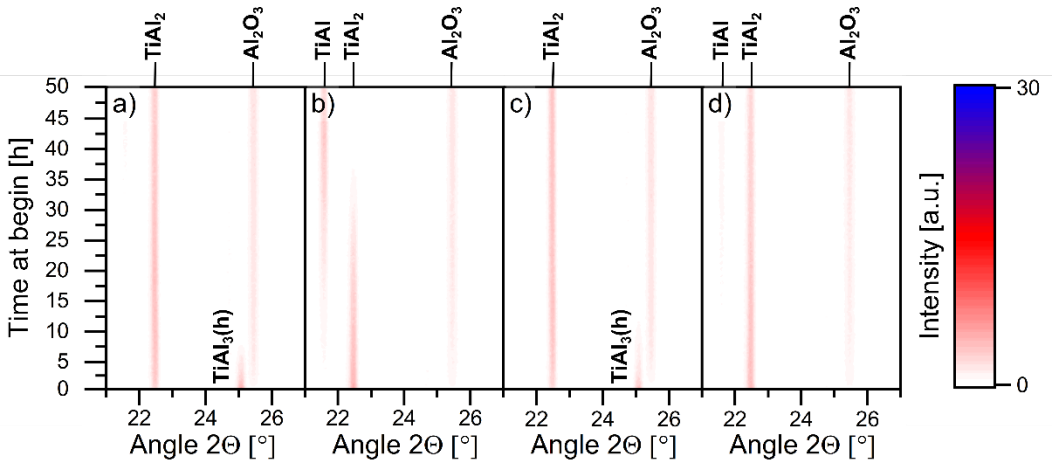

Figure 4: HT-XRD results of the oxidation process to 900 °C. A full scan was performed every 15 minutes and the beginning time is plotted on the ordinate. a) Ti-Si/Al-Ti dual-layer on TNB-V2

substrate, b) single Al-Ti layer on TNB-V2 substrate, c) Ti-Si/Al-Ti dual-layer on TiAl48-2-2 substrate, d) single Al-Ti layer on TiAl48-2-2 substrate

The cross-sectional microstructures of the samples oxidized during the 50 h HT-XRD experiment are presented in **Figure 5** along with EDS line scans. All coated TiAl samples provide a 0.3-0.5 µm thick thermally grown oxide (TGO), consisting of α-Al_2O_3, formed as a continuous and dense layer. The Al content in the Al-Ti top layer is significantly decreased from 60 to about 45 at.% due to the rapid inwards diffusion of Al into the substrate material on the single layer coated TNB-V2 and Ti48-2-2 alloy. The dual layer coated TiAl alloys with the additionally deposited Ti_5Si_3 interlayer exhibit a homogenous Al content of about 60 at.% in the Al-Ti top layer. The Al inwards diffusion was thereby significantly reduced by the Ti_5Si_3 phase at the coating/substrate interfaces. The Al content of 60 at.% indicates that the present phase is $TiAl_2$ whereas a lower Al content of roughly 45 at.% represents γ-TiAl phase. The Ti-Si interlayer is still stable on both dual layer coated TiAl alloys after 50 h of exposure to 900 °C. The thickness of the interlayer (approx. 1.2 µm) remained unchanged. However, the morphology changed from initial columnar structure to a dense layer enclosing oxide intrusions. The dark oxide precipitates of alumina at the coating/substrate interface are most likely remnants of the EDM sample preparation as already seen in the as-deposited condition in Figure 1.

Above and below the Ti_5Si_3 interlayer, small bright precipitates less than 100 nm in diameter were formed, but could not be clearly identified by SEM. In the TNB-V2 sample, the number of precipitates above and below the interlayer seems to be comparable. In contrast, in the TiAl48-2-2 sample a higher number of precipitates were present above the interlayer. Therefore, detailed TEM investigations were performed and are presented in the section 3.2.

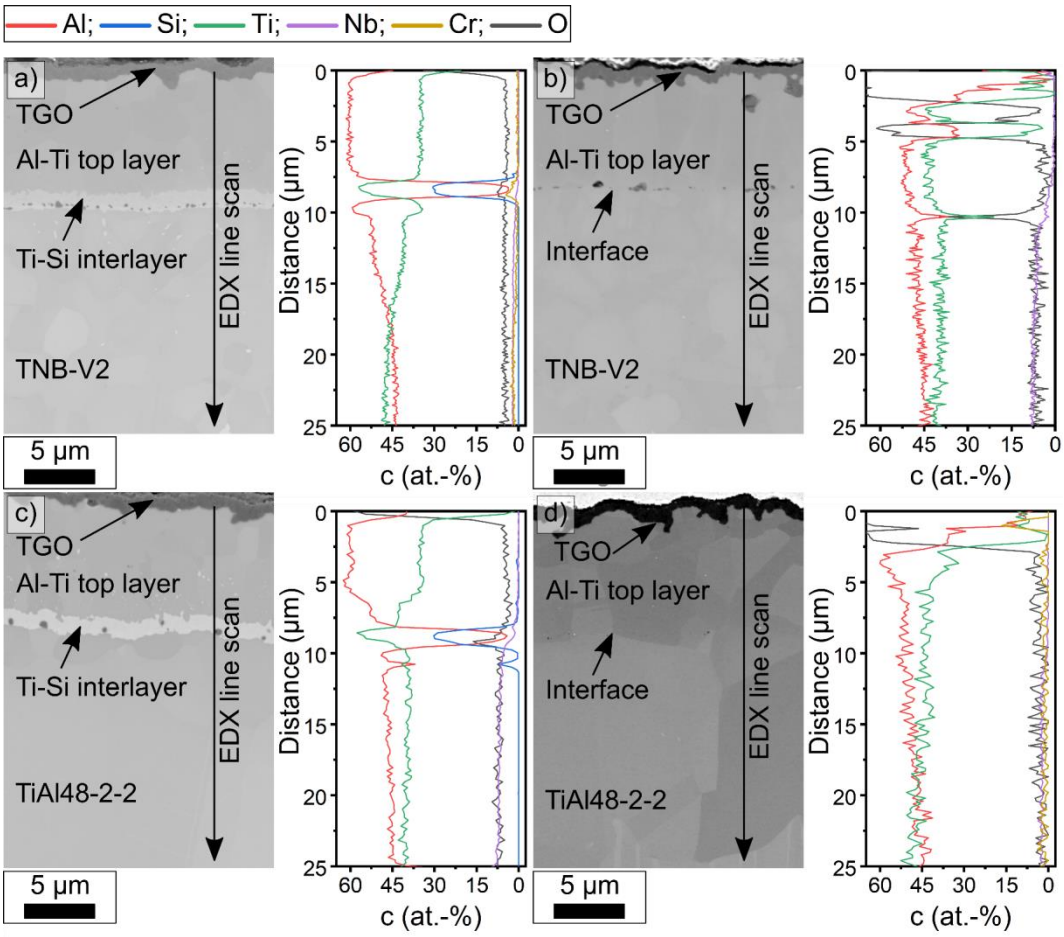

Figure 5: SEM cross sections of different samples after 50 h of oxidation during the HT-XRD measurement with the associated EDX line scans in at.%. a) Al-Ti/Ti-Si dual-layer on TNB-V2 substrate, b) single Al-Ti layer on TNB-V2 substrate, c) Al-Ti/Ti-Si dual-layer on TiAl48-2-2 substrate, d) single Al-Ti layer on TiAl48-2-2 substrate.

3.2. Oxide formation, microstructure and diffusion processes after short time exposure of 10 cycles to 900°C

The single as well as the dual layer coated TNB-V2 and TiAl-48-2-2 alloy were cyclic oxidation tested at 900°C in laboratory air without any post-heat treatment. After 10 cycles of exposure, the dual layer coated TNB-V2 and Ti48-2-2 alloys formed a plate-like oxide (see SEM top view images in **Figure 6**a and c), whereas on the single layer coated TiAl samples only very isolated plate-like oxides were visible (Figure 6b, d). Instead of the plate-like oxides, a dense and smoother oxide layer formed on the single layered samples. Gauthier et al. [11] observed in their study a plate-like oxide

formation on pure $TiAl_3$ coatings that was found to be the θ-Al_2O_3 oxide. In comparison to $TiAl_3$, $TiAl_2$ formed α-Al_2O_3 oxide during oxidation at 900°C [11]. In XRD, no θ-Al_2O_3 was identified which could be the result of its too small dimensions. However, the SEM top view images in Figure 6 clearly showed the different morphology of the formed oxides. Moreover, it has been found that in the case of Ni-base superalloys the plate- or whisker-like morphology doesn't necessarily indicate the presence of transient alumina polymorphs since a transformation to the stable α-Al_2O_3 could have already took place [35].

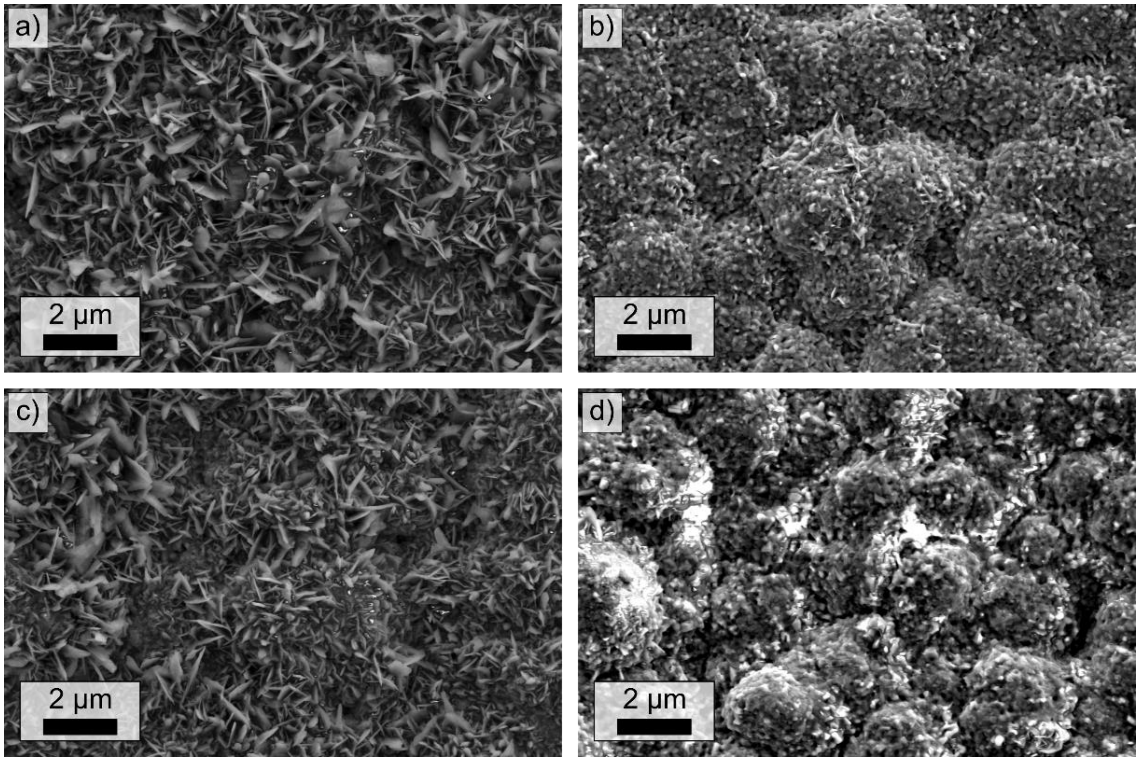

Figure 6: Top view SEM images of coatings after 10 cycles of oxidation at 900°C: a) dual layer coated TNB-V2, b) single layer coated TNB-V2 alloy, c) dual layer coated Ti48-2-2 alloy, d) single layer coated Ti48-2-2 alloy

Cross sections of the coated samples after the 10 cycles of cyclic oxidation at 900°C were prepared and studied by SEM (**Figure 7**). On top of the samples a TGO layer formed which mainly consisted of Al and O, which is in line with the HT-XRD

results that showed the presence of mainly α-Al_2O_3 (Figure 4). Below the TGO, all Al-Ti coatings were depleted in Al and thus its content decreased from 70 at.% in the as deposited condition to around 60 at.% Al after 10 cycles.

In case of the dual layer coated TNB-V2 samples, the region above the Ti_5Si_3 interlayer consisted solely of the $TiAl_2$ phase, which was identified by EDX (Figure 7a) and proven by select area diffraction (SAD) using TEM (**Figure 8**a).

For the dual layer coated TiAl48-2-2 sample (Figure 7c), the Al depletion took place in two regions: in the top region of the coating, due to Al_2O_3 formation, and close to the Ti_5Si_3 interlayer, where minor inward Al diffusion led to its marginal depletion. Based on SEM-EDX (Figure 7c), in the middle of the top layer the Al content of roughly 70 at.% was found, indicating the presence of $TiAl_3$. Below the TGO and above the interlayer around 60 at.% of Al suggest the presence of $TiAl_2$. However, TEM results revealed that above the interlayer $TiAl_3$ was also present (**Figure 9**a). This discrepancy could be a result of the SEM-EDX measurement which excites a larger volume below the surface and provides averaged results.

In both dual layered samples, the Ti-Si interlayer eventually formed Ti_5Si_3 without amorphous regions after 10 cycles of oxidation at 900°C (Figure 8b and Figure 9b). The absence of the Ti_5Si_3 associated peaks in XRD (compared to **Figure 16**) allows for the conclusion that the Al-Ti top layer is too thick to be completely penetrated by the X-ray, therefore Ti_5Si_3 cannot be detected by XRD. In case of the TNB-V2 substrate, some $TiAl_2$ formed below the Ti_5Si_3 interlayer which merges into an Al-rich TiAl layer (Figure 8c, d). In contrast, only Al-rich TiAl was present below the interlayer in the TiAl48-2-2 sample (Figure 9c, d).

In the single layer coated samples, the Al depletion was more pronounced leading to a complete transformation of $TiAl_3$ to $TiAl_2$ (60 at.%) and further to TiAl

(~45 at.%). This indicates a faster Al diffusion compared to the dual layered samples. As observed after 50 h of isothermal oxidation at 900 °C (Figure 5), bright precipitates already formed after 10 cycles above and below the Ti_5Si_3 interlayer. In the TNB-V2 sample these precipitates were present above and below the interlayer. In contrast, for the TiAl48-2-2 sample the precipitates are present above the interlayer.

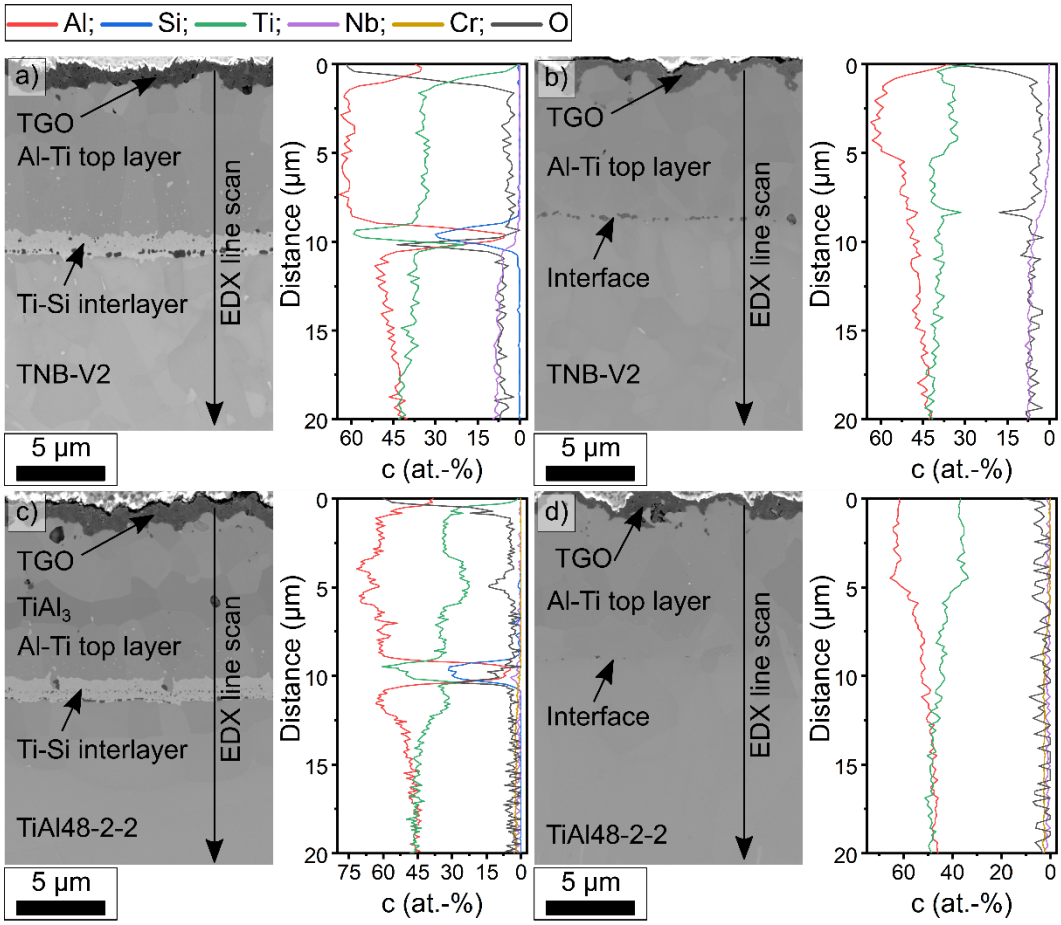

Figure 7: SEM cross sections of different samples after 10 cycles of oxidation with the associated EDX line scans. a) Ti-Si/Al-Ti dual-layer on TNB-V2 substrate, b) single Al-Ti layer on TNB-V2 substrate, c) Ti-Si/Al-Ti dual-layer on TiAl48-2-2 substrate, d) single Al-Ti layer on TiAl48-2-2 substrate

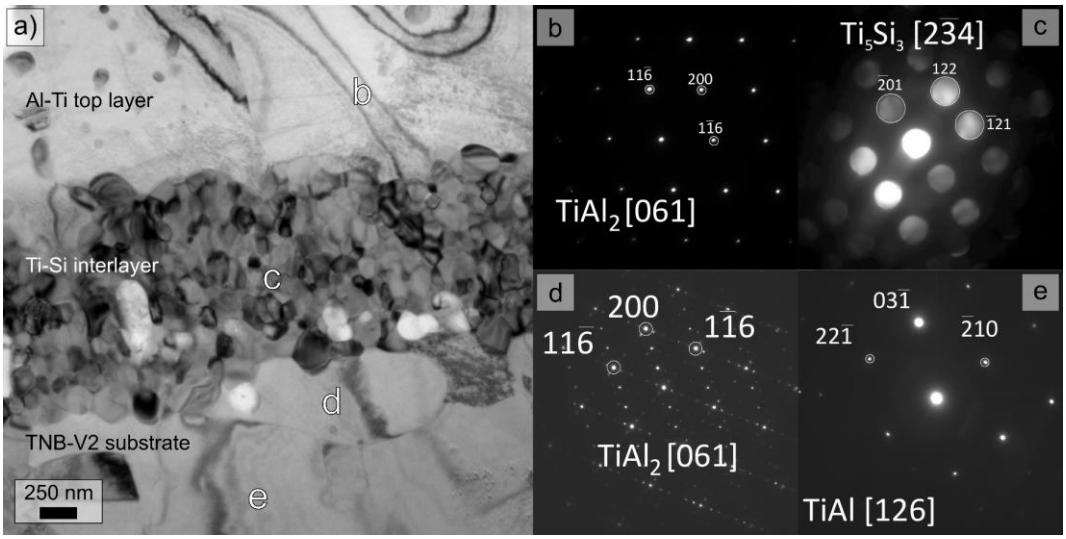

Figure 8: TEM analysis of the Ti-Si/Al-Ti dual-layer on TNB-V2 substrate after 10 1h-cycles at 900°C: a) BF image and selected area diffraction patterns of the areas marked as b-e.

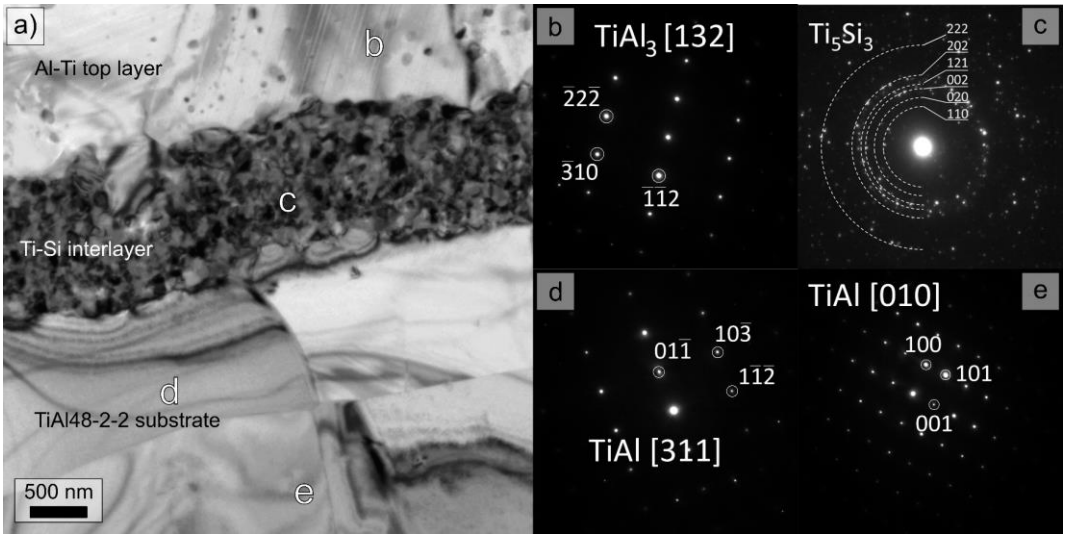

Figure 9: TEM analysis of the Ti-Si/Al-Ti dual-layer on TiAl48-2-2 substrate after 10 1h-cycles at 900°C: a) BF image and selected area diffraction patterns of the areas marked as b-e.

Additional STEM analyses were performed after 10 cycles of oxidation to provide a more detailed understanding of the diffusion processes. The elemental mapping of the whole interlayer on the TNB-V2 sample shows a homogeneous distribution of Ti and Si (**Figure 10**a). In contrast, Al is mainly present within the oxide particles, which are the residues of EDM, as well as in the substrate and top layer. However, the Nb content seemed to gradually reduced within the interlayer from the

Nb-containing substrate alloy to the Al-Ti top layer. At a higher magnification of the interlayer segregation of Nb and Al to the grain boundaries is visible (Figure 10b).

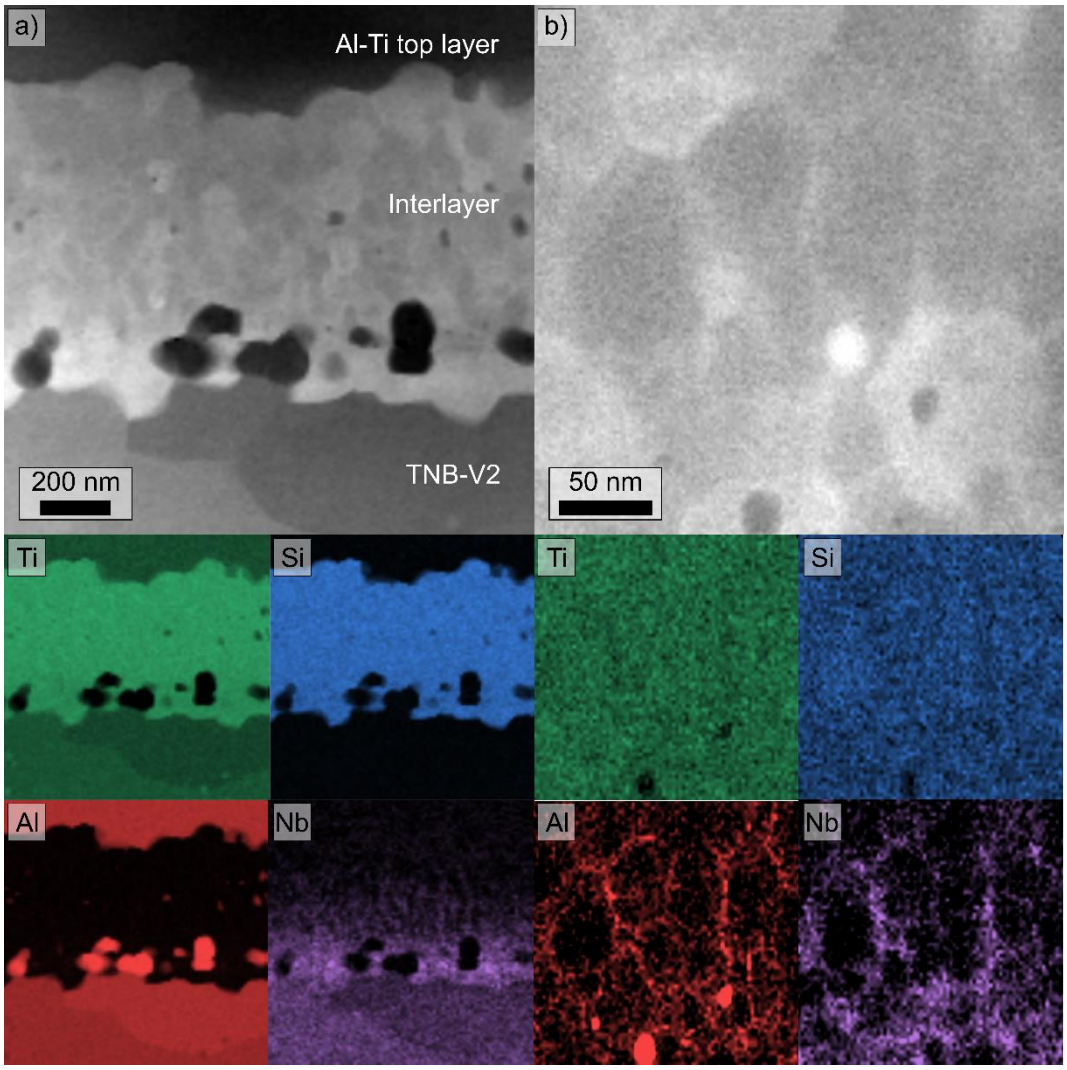

Figure 10: STEM EDX mapping of two different regions of the Ti_5Si_3 interlayer on TNB-V2 substrate after 10 1h-cycles at 900°C with two different magnifications: a) the whole Ti_5Si_3 interlayer b) a higher magnification of the Ti_5Si_3 interlayer

In the Ti_5Si_3 interlayer on the TiAl48-2-2 substrate a homogenous distribution of Ti and Si as well as Al-rich oxide particles are also present (**Figure 11**a). However, Nb is predominantly present in the substrate and appears to have been blocked from diffusing into the interlayer. In comparison, Cr is found throughout the interlayer and accumulated mainly at the substrate/interlayer and interlayer/top layer interfaces. At

higher magnification of the interlayer, it is also clear that Cr segregates preferentially at the grain boundaries (Figure 11b). A slight segregation of Al along the grain boundaries can be also seen, nevertheless, Al is also present within the Ti_5Si_3 grains. Nb is relatively homogeneously distributed in the interlayer and no distinct segregation is visible.

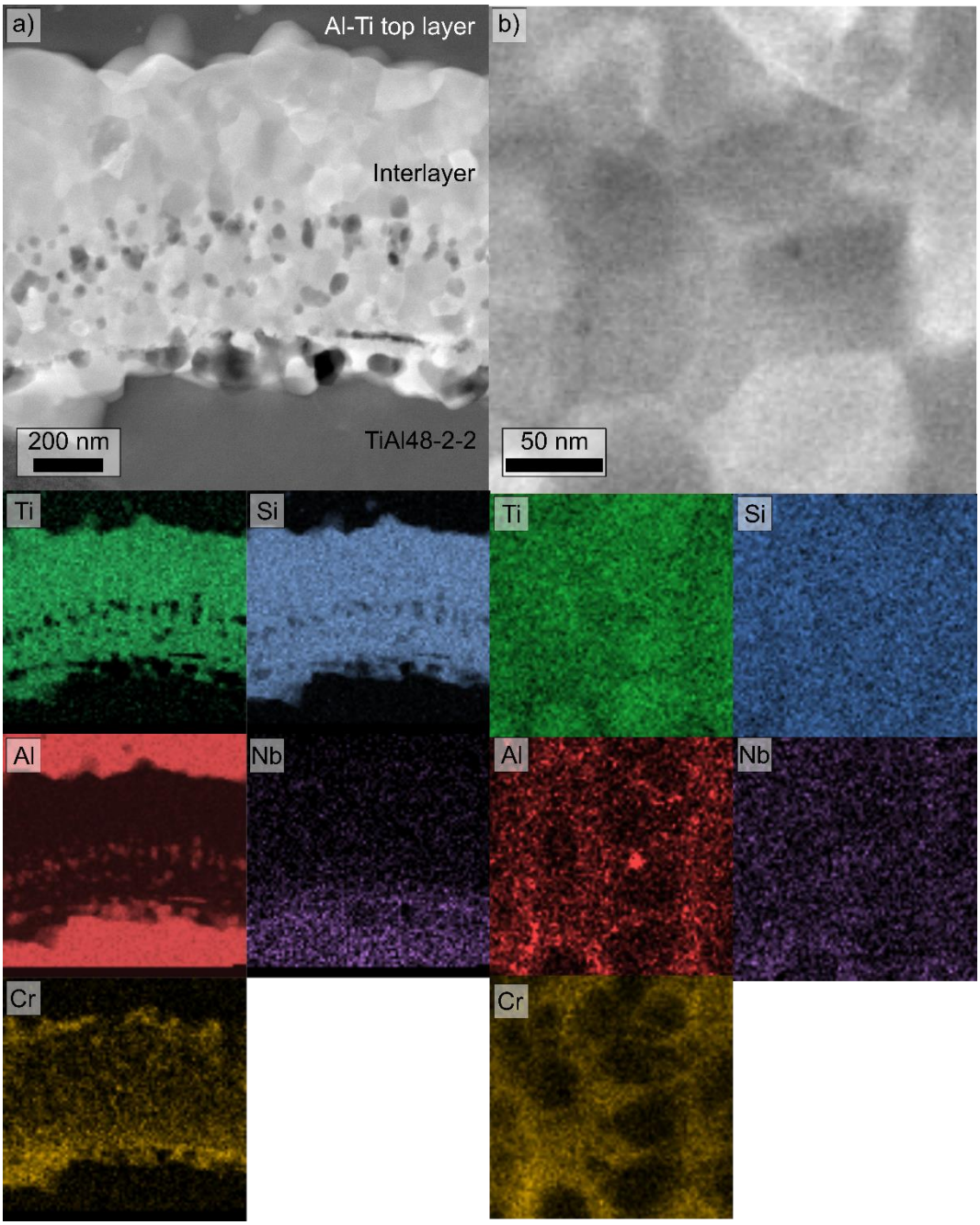

Figure 11: STEM EDX mapping of two different regions of the Ti_5Si_3 interlayer on TiAl48-2-2 substrate after 10 1h-cycles at 900°C with two different magnifications: a) the whole Ti_5Si_3 interlayer b) a higher magnification of the Ti_5Si_3 interlayer

The precipitates which formed close to the interlayer during oxidation were studied using TEM and EDS (**Figure 12** and **Table 1**). The region without the precipitates, above the interlayer, mainly consists of Al and Ti with only minor amounts of Si and no Cr or Nb (Point 1). Directly below the interlayer, an Al rich region is present (64 at.%, Point 2) followed by a region with a lower Al content (53.9 at.%, Point 3). Due to the inward diffusion of Al from the Al-Ti top layer to the substrate the content of the alloying elements, Cr and Nb, is lower than in the unaffected substrate. However, the Cr content is reduced more than the Nb content, while Si was not found below the interlayer. The precipitates, which formed only above the interlayer on the TiAl48-2-2 substrates are rich in Si, contain some Cr and no Nb (Points 4-9). Due the small dimensions of the precipitates the EDS measurements are affected by the surrounding area. However, it can be assumed that these precipitates are silicides due to the high Si content.

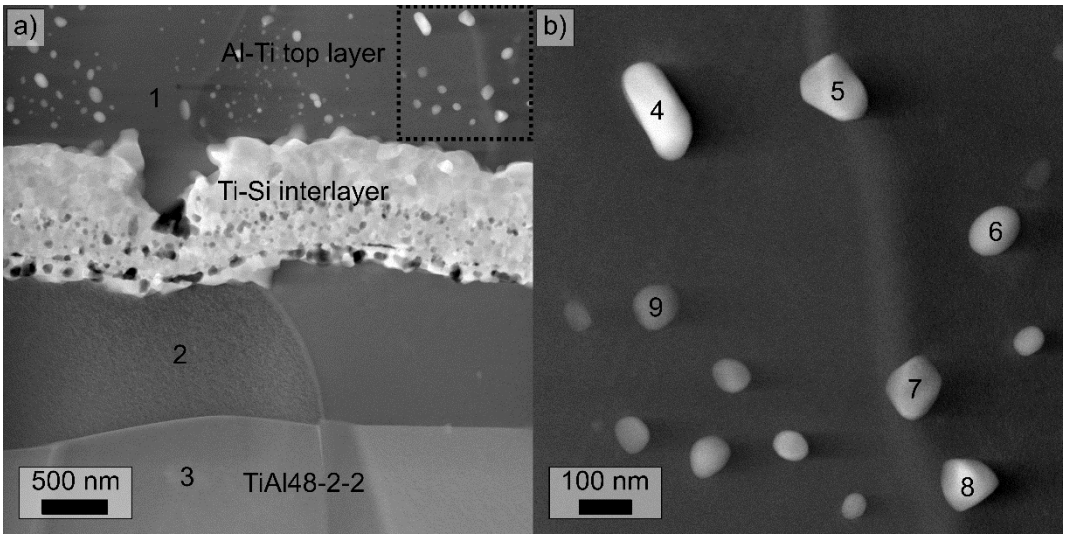

Figure 12: HAADF images of the dual layer coated TiAl48-2-2 substrate after 10 1h-cycles at 900°C in TEM with EDS point analysis: a) region around the interlayer on a TiAl48-2-2 sample, b) higher magnification of the precipitates

Table 1 EDS point measurements of the marked points in Figure 12

Point	Al [at.%]	Ti [at.%]	Si [at.%]	Cr [at.%]	Nb [at.%]
1	69.5	29.7	0.8	0.0	0.0
2	64.0	33.5	0.0	0.5	2.0
3	53.9	41.2	0.0	1.7	3.2
4	13.1	56.2	27.8	2.8	0.0
5	36.8	47.4	13.4	2.4	0.0
6	27.8	45.6	21.4	5.2	0.0
7	40.8	43.1	14.0	2.2	0.0
8	34.5	48.1	16.1	1.2	0.0
9	52.7	39.9	5.6	1.9	0.0

3.3. Long-term cyclic oxidation behavior at 900 °C up to 1000 1 h cycles

Cyclic oxidation tests were performed at 900 °C in laboratory air for a total of 1000 cycles with 1 h heating and 10 minutes cooling period. Based on these tests the mass changes versus the number of 1h-cycles were prepared and are shown in **Figure 13**. The TNB-V2 as well as the Ti48-2-2 alloy coated with the dual layer system, consisting of Al-Ti top and Ti-Si interlayer, provides a parabolic growth rate up to the maximal tested time of 1000 1h-cycles at 900°C. Also, the single layer coated Ti48-2-2 alloy without the Ti_5Si_3 interlayer exhibits a good oxidation behavior due to a parabolic growth rate up to 1000 cycles. The maximal mass gain of both single- and double-layer coated Ti48-2-2 alloy as well as of the double-layer coated TNB-V2 alloy stayed below 1 mg/cm² after 1000 cycles of oxidation. The calculated parabolic rate constants K_p, are listed in **Table 2**. The Al-Ti single layer coated TNB-V2 alloy shows a parabolic progression up to 780 1h-cycles at 900°C. At further cyclic exposure the TNB-V2 alloy without Ti_5Si_3 interlayer deviates from this progression by showing a linear trend. At the same time of 780 cycles, bright yellow spots formed on the surface, indicating the formation of TiO_2 due to significant consumption of Al in the coating.

Overall, the growth constants K_p of the dual layer coated samples are lower than those of the single layer coated samples. Interestingly, during the first 250 cycles the single layered samples showed a lower mass gain whereas at higher amounts of cycles the dual layered samples exhibited lower mass changes. This phenomenon took place on both coated TiAl substrates at the same time. The sporadic mass loss of the coated samples is due to spallation of the oxide layer mainly at the edges and less protected side surfaces, but did not cause a major damage. In comparison, the uncoated TNB-V2 and TiAl48-2-2 substrates shows a high, linear mass increase up to more than 1.25 mg/cm² after just 100 cycles followed by a rapid mass decrease due to spallation.

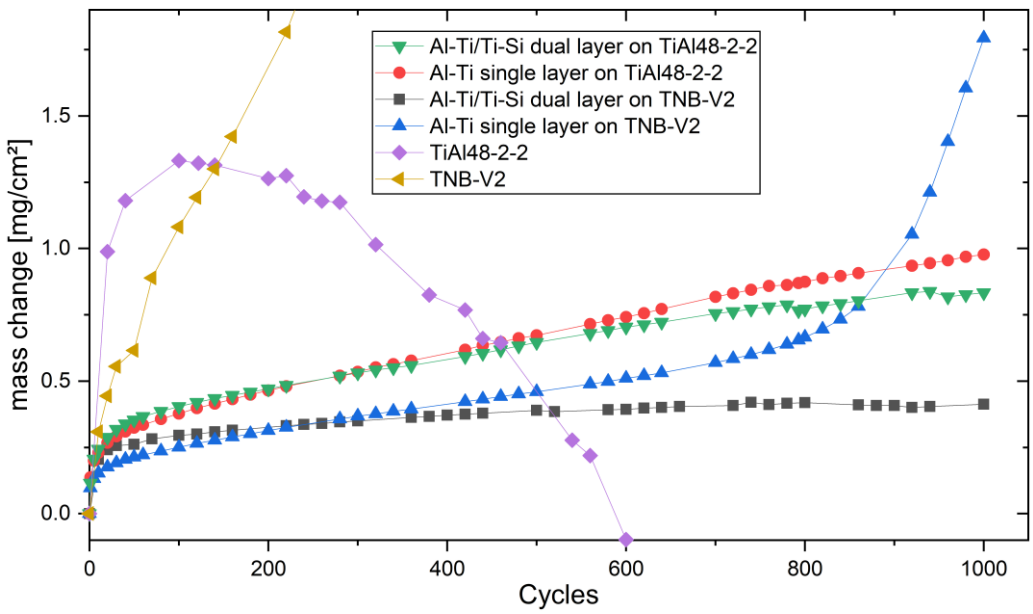

Figure 13: Mass change over cycle amounts of the bare, single- and double layer coated TNB-V2 and TiAl48-2-2 alloys during exposure to 900°C in laboratory air.

Table 2: Parabolic rate constants Kp of the different coatings in $mg^2/(cm^4h)$ determined from the cyclic oxidation test and calculated by the method suggested by Pieraggi [36]

	TNB-V2 [mg^2/cm^4h]	TiAl48-2-2 [mg^2/cm^4h]

Dual layer	5.9×10^{-5}	38.9×10^{-5}
Single layer	28.6×10^{-5}	57.1×10^{-5}

The cyclic oxidation tests up to 1000 cycles at 900°C led to the formation of TiO_2 oxide nodules in the single layer coated TNB-V2 samples indicating the failure of the Al-Ti coating (**Figure 14**). EDX mappings revealed that Ti-rich regions are present in the intact area below the TGO indicating the presence of Ti-rich phases of probably Ti_3Al or $Ti_5Al_3O_2$ Z-phase. However, for the Z-phase a higher O content in the Ti-rich regions would be expected.

The SEM images of the remaining samples, the dual layer coated TNB-V2 and TiAl48-2-2 as well as the single layer coated TiAl48-2-2 alloy (**Figure 15**a, c, d), showed only minor differences in the microstructure in comparison with the microstructure after 10 cycles of exposure to 900°C (see Figure 7). EDS line scans also revealed the further reduction of the Al-content to below 50 at. %, which indicates the presence of the γ-TiAl phase. However, the Ti_5Si_3 interlayers were still clearly visible and maintained the same thickness even after the 1000 cycles of oxidation on the TNB-V2 as well as on the TiAl-48-2-2 alloy. Also, the Si-rich bright precipitates of probably Ti_5Si_3, which were already present after 10 cycles of oxidation, are still visible after 1000 cycles.

In terms of diffusion, the alloying elements - Cr and Nb, showed a different behavior. In the dual layer coated TNB-V2 sample, the Nb content decreased rapidly within the Ti_5Si_3 interlayer and then decreased further in the top layer (Figure 15a). However, right below the TGO the Nb content increased again. For the TNB-V2 sample without a Ti_5Si_3 interlayer the Nb content also decreased within the top layer, but was slightly enlarged below the TGO (Figure 15b). In the TiAl48-2-2 samples, the Nb

content in the Ti_5Si_3 interlayer as well as the Al-Ti top layer in both samples was very low (<1 at.%) and not clearly determinable, probably because of the minor initial Nb-content in the TiAl-48-2-2 alloy of 2 at.%. In contrast, Cr accumulated within the Ti_5Si_3 interlayer and was present in the Al-Ti top layer of both the dual as well as the single layer coated TiAl48-2-2 samples. The low Cr content makes its clear determination difficult but it seemed it has been balanced out in the top layer and corresponded approximately to the Cr content of the substrate material of 2 at.%. It is already known that Cr has a higher diffusion coefficient in TiAl than Nb. [37] However, the results in this paper suggest that Cr could hinder the Nb diffusion in the Al-Ti top layer.

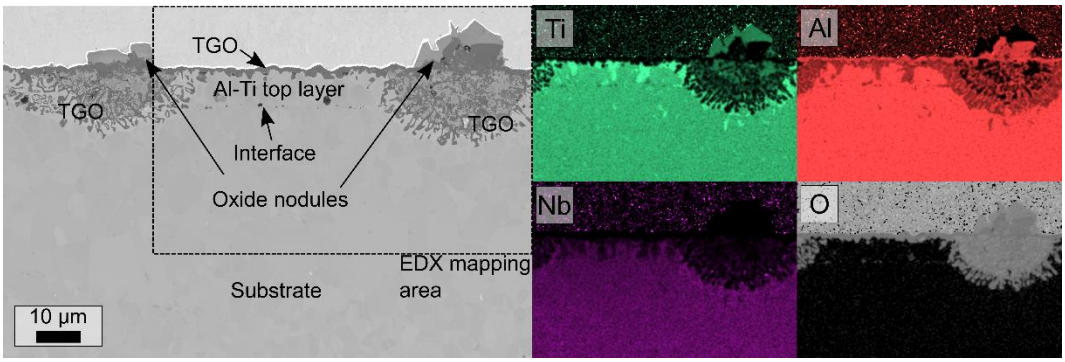

Figure 14: SEM cross section of a single layer coated TNB-V2 alloy after 1000 cycles of oxidation with corresponding EDX mappings

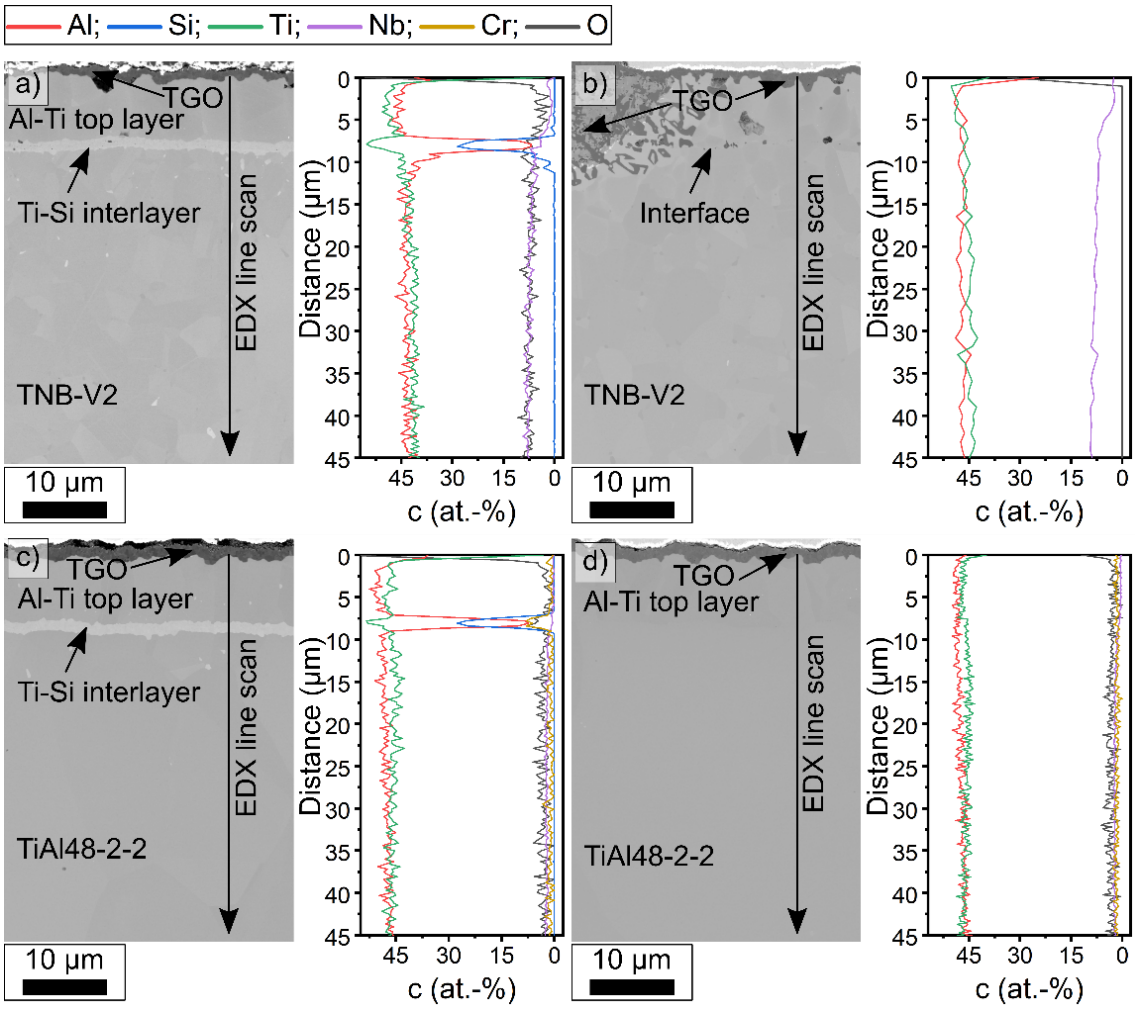

Figure 15: SEM cross sections of different samples after 1000 cycles of oxidation with the associated EDX line scans. a) Ti-Si/Al-Ti dual-layer on TNB-V2 substrate, b) single Al-Ti layer on TNB-V2 substrate, c) Ti-Si/Al-Ti dual-layer on TiAl48-2-2 substrate, d) single Al-Ti layer on TiAl48-2-2 substrate

Finally, XRD measurements were performed at room temperature after various amounts of cycles to study the phase transformations during the cyclic oxidation tests at 900°C. In Figure 16, sections of the x-ray diffractograms of each single and double layer coated TiAl-based alloys after 10, 50, 100, 500 and 1000 cycles are presented, respectively. In the dual layer coated TNB-V2 sample (Figure 16a), no peaks of the $TiAl_3$ phase were observed after 10 cycles of oxidation to 900°C. The $TiAl_2$ peaks disappeared completely after 500 cycles. Simultaneously, the intensity of the γ-TiAl phase reflexes increased, indicating the transformation of $TiAl_2$ to γ-TiAl. In

comparison, in the diffractogram of the single Al-Ti layer coated TNB-V2 substrate (Figure 16b), the $TiAl_2$ peaks were no longer visible after 50 cycles.

In case of the double layer coated TiAl48-2-2 substrates (Figure 16c), the $TiAl_3$ phase was still present after 10 cycles and disappeared during further oxidation. The $TiAl_2$ phase maintained over 500 cycles and its peaks vanished completely after 1000 cycles. In the single Al-Ti coated TiAl48-2-2 (Figure 16d), the disappearance of the $TiAl_2$ phase occurred already between 100 and 500 cycles. The oxide scale that formed during the test was found to be mainly composed of α-Al_2O_3. Just the single layer coated TNB-V2 samples show significant reflexes of TiO_2 after 1000 cycles.

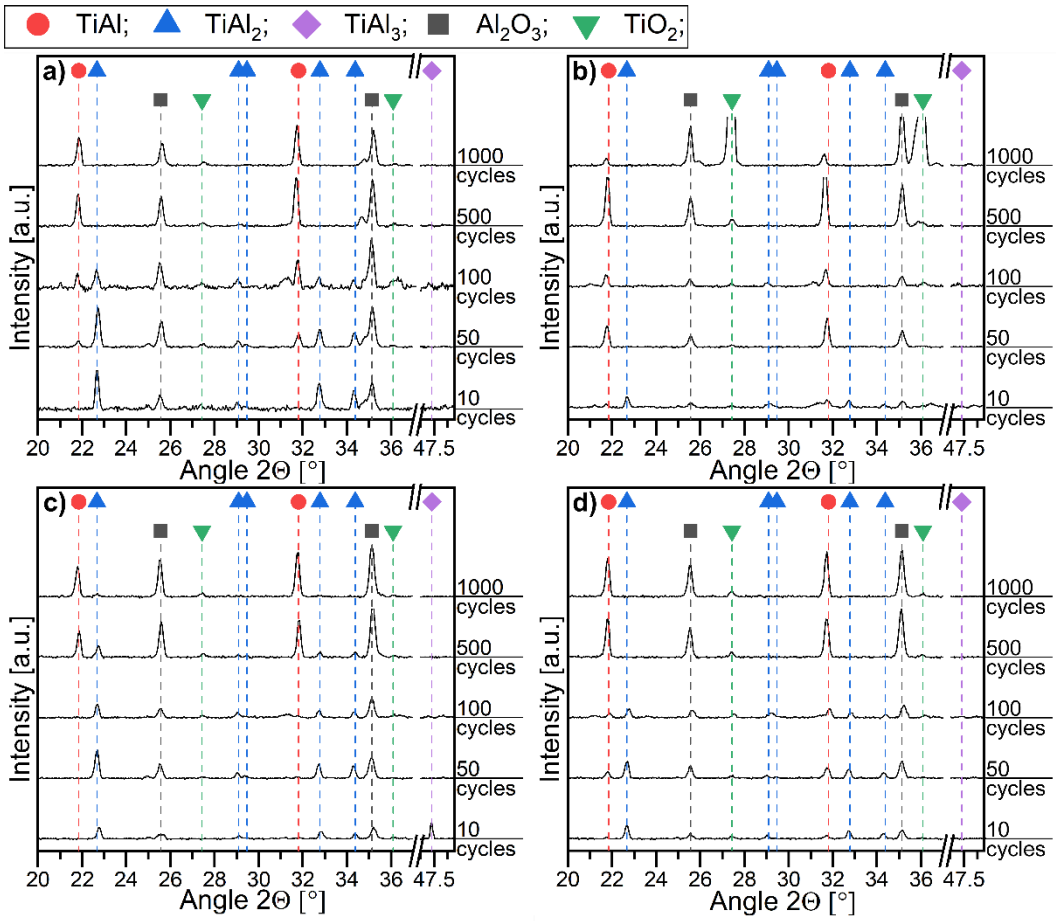

Figure 16: XRD measurements after 10, 50, 100, 500 and 1000 oxidation cycles at 900 °C. a) Ti-Si/Al-Ti dual-layer on TNB-V2 substrate, b) single Al-Ti layer on TNB-V2 substrate, c) Ti-Si/Al-Ti dual-layer on TiAl48-2-2 substrate, d) single Al-Ti layer on TiAl48-2-2 substrate

4. Discussion

4.1. Behavior of the coatings after the deposition process as well as during the initial high temperature exposure

The deposition of a double-layered system of a Ti-Si interlayer and Al-30Ti top layer using a one-batch magnetron sputtering process (in at.%) was successfully demonstrated within this work. The coating system showed an excellent adhesion on both tested γ-TiAl substrates, TNB-V2 and TiAl48-2-2. The coating microstructure of the Al-Ti top layer belongs to zone 3 according to the Thornton model [38], providing a homogenous and dense microstructure (Figure 1). This indicates a high proportion of the deposition temperature (T_s=723,15 K) and the melting point (T_m) of the top layer. However, according to Schuster and Palm the melting point of $TiAl_3$ and Ti_5Al_{11} is in the range of 1673.15 K and 1723.15 K [39]. With this melting range the T_s/T_m proportion would be around 0.43 leading to a structure according to zone 1 or T. In comparison, the T_s/T_m ratio for pure Al (T_S= 938,15 K) is 0.77. This suggests that Al and Ti is co-deposited but not reacted immediately after the condensation at the substrate but with a certain delay. During this time period, the high mobility of Al allowed to form a dense layer due to surface diffusion. Thus, the microstructure according to zone 3 formed. The interlayer of Ti_5Si_3 showed a columnar coating morphology in accordance with zone 1 of the model by Thornton, due to a much lower T_s/T_m proportion for Ti_5Si_3 as well as for Ti and Si. Directly after the deposition process, the Al-Ti top layer as well as the main area of the Ti-Si interlayer exhibit a mostly crystalline microstructure (Figure 2), which is not commonly observed for magnetron sputtering processes due to low substrate temperatures [40]. Therefore, the potential volumetric reduction accompanying the crystallization of the amorphous regions during the initial heating-up period is omitted, which could result in less

sensitivity for cracking and an improved adhesion between the coating and substrate materials as well as between the two layers.

The Al-30Ti top layer consisted predominantly of the metastable Ti_5Al_{11} phase with some minor part of the $TiAl_3$ phase. At about 660°C the complete transformation of the Ti_5Al_{11} phase to the expected $TiAl_3$ and $TiAl_2$ was confirmed by *in situ* HT-XRD (Figure 3). The application of this coating for oxidation protection of TiAl-based alloys, which are commonly operating at temperatures around 750°C and slightly above, seems possible. Moreover, the HT-XRD measurements of the dual layer coated TiAl-based alloys confirm the higher stability of the $TiAl_3$ phase in the presence of the Ti_5Si_3 interlayer (Figure 4), which results in a higher Al-content in the coating. SEM analysis of the cross sections of the coated substrates (Figure 5) confirms the higher Al-content in the top layer in the presence of a Ti_5Si_3 interlayer after 50 h of oxidation at 900 °C. Just a minor reduction of the initial Al-content of 70 at% to 60 at.% was confirmed by EDS line scans.

4.2. Diffusion processes in Ti_5Si_3 and its potential as diffusion barrier for Al on TiAl-based alloys

The results in the present work demonstrate the Al diffusion hindering properties of the Ti_5Si_3 interlayer on TiAl-based alloys. The coating systems with a Ti_5Si_3 interlayer maintained the Al-rich $TiAl_3$ and $TiAl_2$ phases around 5-10 times longer than the single Al-Ti coated TiAl alloys (Figure 16). Moreover, the $TiAl_3$(h) phase was not observed in the single Al-Ti top layer (Figure 4). According to Braun and Ellner, the transition temperature of the two $TiAl_3$ polymorphs ($TiAl_3$(h) and $TiAl_3$(l)) is strongly influenced by the Al content and varies from 735 °C for the Al-rich $TiAl_3$ to roughly 900 °C for the Ti-rich one [41]. Therefore, it can be concluded that the fast Al diffusion between the single Al-Ti top layer and the substrate occurred already during the short period of heating during the HT-XRD measurement, roughly 20 minutes.

In order to find a possible approach to explain the diffusion-inhibiting properties of the Ti_5Si_3 phase, a fundamental understanding of the involved processes is required. Diffusion in solid states could take place through the lattice (bulk diffusion) or along the grain boundaries. It is commonly well known that grain boundary diffusion is much faster than bulk diffusion. However, the volume fraction of grain boundaries is usually low compared with the volume fraction of bulk grains. Therefore, the total diffusion flux at the grain boundaries does not necessarily exceed the volume diffusion flux.

To allow bulk diffusion in Ti_5Si_3, Al needs to be dissolved in this intermetallic phase. This happens by substituting Si to form $Ti_5(Al,Si)_3$ [42, 43]. While the maximum solubility of Al in Ti_5Si_3 is around 8 at.% [44], de Farias Azevedo et al. found that its concentration at 900 °C is around 3 at.% [42].

In this work, the different phases in the Al-Ti top layer were formed by solid state reaction of the elements during initial oxidation at 900 °C. During oxidation, the top layer consisted of the $TiAl_3$, $TiAl_2$ and γ-TiAl phases. Except for $TiAl_3$, these phases have a low solubility of Si (maximum of 0.5 at.%) [21, 44]. Thus, the rejection of Si from the Ti_5Si_3 to the $TiAl_2$ or γ-TiAl phase leads to a phase formation. To illustrate this, thermodynamic calculations using the Thermo-calc software [45] and TCTI2 Ti/TiAl-alloys database version 2.2 were utilized to calculate the phase development when Si is dissolved in $TiAl_3$, $TiAl_2$ and TiAl (**Figure 17)**. The calculations show that already very small amounts of Si (0.05 at.%) provoke a Ti_5Si_3 formation in γ-TiAl. The same behavior occurs for $TiAl_2$ where Ti_5Si_3 and $TiAl_3$ form once the total Si content increases above 0.05 at.% and 0.63 at.%, respectively. In contrast, $TiAl_3$ can solve up to 16.4 at.% of Si [46] and thus no phase formation takes place at lower Si contents. Therefore, the dissolving of Al in Ti_5Si_3 seemed to be thermodynamically hindered when Ti_5Si_3 is adjacent to TiAl and $TiAl_2$. As a result, a very low amount of Al is

dissolved in the Ti_5Si_3 interlayer which would only allow a minor lattice diffusion flux. Furthermore, there is no data in the literature on the diffusion of Al in the Ti_5Si_3 phase or in general self-diffusion of Al and Si in $Ti_5(Al,Si)_3$ due to the lack on suitable tracers for Al and Si [47]. Additionally, the diffusion in intermetallic phases is more complex than in dilute alloys due to their highly ordered structure [47]. These reasons make it additionally difficult to form a statement on the Al bulk diffusion in Ti_5Si_3.

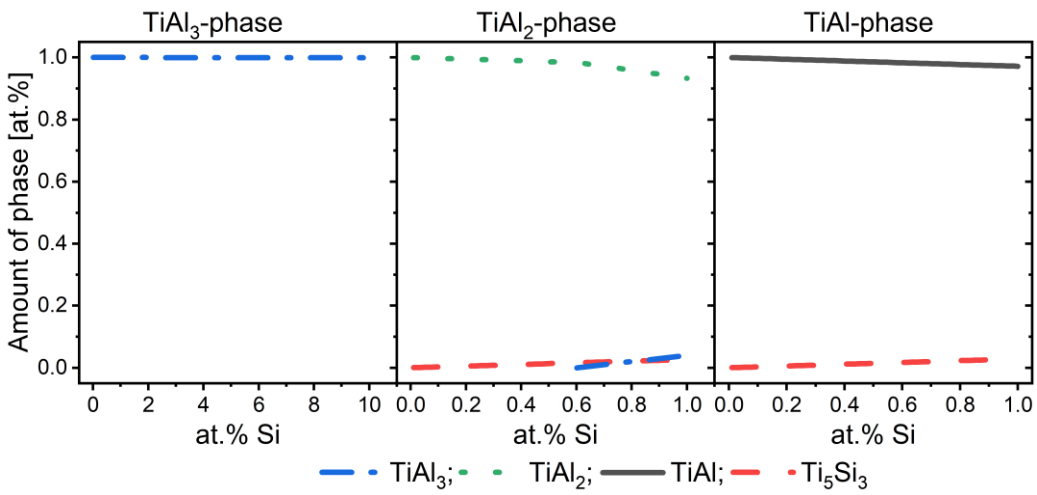

Figure 17: Thermodynamic calculations of the phase fraction of $TiAl_3$, $TiAl_2$ and γ-TiAl phases with increasing Si content at 900 °C.

In this study, TEM analysis showed a strong segregation of Al along the grain boundaries of the Ti_5Si_3 interlayer (Figure 10 and Figure 11). This suggests that grain boundary diffusion is the important factor for the Al depletion in the Al-Ti top layer. Apart from the segregation of Al, the alloying elements such as Nb and Cr segregated to the grain boundaries of the Ti_5Si_3 layer as well. A basic attempt to characterize grain boundary diffusion kinetics can be done by the Harrison's Classification [48]. For example, type C kinetics occur when the diffusion takes place along the grain boundaries without any significant bulk diffusion [48]. On the other hand, type B kinetics take place when a certain amount of bulk diffusion occurs and thus the

diffusing atoms can enter into the grains [48]. Interestingly, the grain boundary diffusion in the interfaces on the different substrates can be characterized as different types. The interlayer on the Nb-containing TNB-V2 substrate has more characteristics of type C kinetics whereas on the Cr- and Nb-containing TiAl48-2-2 substrate the kinetics are closer to type B.

The alloying elements, such as Nb in the TNB-V2 alloy and Cr in TiAl48-2-2 alloy exhibit the same types of diffusion kinetics as Al, which allows the assumption that they affect it. Nb was found to diffuse along the grain boundaries but did not penetrate the entire interlayer (Figure 10). In contrast, Cr was found at the interlayer/top layer interface and therefore penetrated it entirely. In addition, Cr entered the grains from the grain boundaries implying a certain amount of bulk diffusivity. This allows the conclusion that Cr can diffuse faster in the interlayer than Nb. The reason for this could be the smaller atomic radius of Cr but also different reactions at the grain boundaries, such as segregation and phase formation. However, this requires further investigations. With regard to Al diffusion, there is an opposite trend depending on the element. In the Nb-containing TNB-V2 alloy the depletion of Al in the top layer took place faster than in the Cr-containing TiAl48-2-2 alloy. This is especially worth mentioning, since Cr at the grain boundaries leads to a broader diffusion front, but not to a higher flux of Al. In the absence of a direct comparison with an interlayer on a pure TiAl substrate it cannot be clearly determined whether the Cr or Nb segregation has a positive or negative influence on Al diffusion. However, on the basis of the available results, it can be assumed that Nb, compared to Cr, could enhance the Al diffusion along the grain boundaries. The description of an exact mechanism however requires further investigations.

Another point that requires discussion is the long-term stability of the Ti_5Si_3 interlayer. It was shown that even after 1000 h of oxidation at 900 °C, the interlayer is still present almost unchanged with the initial thickness of 1.2 µm. This is also due to the low solubility of Si in the γ-TiAl and $TiAl_2$ phases which suppresses the Si dissolving in the top layer as well as in the substrate alloys. However, during the initial oxidation, $TiAl_3$ is still present adjacent to the Ti_5Si_3 interlayer. Due to the high solubility of Si in $TiAl_3$ some of the Si diffuses from the Ti_5Si_3 phase to the $TiAl_3$ phase. When the Al content in the Al-Ti top layer decreases, $TiAl_2$ starts to form therefore the dissolved Si is rejected and Ti_5Si_3 precipitates are formed. This mechanism was already described in a previous work [21] and explains the formation of the bright Si-rich precipitates above the interlayer (Figure 12).

In any case, in both coated TiAl alloys, TNB-V2 as well as TiAl48-2-2, the Al depletion was reduced in comparison to the samples without a Ti_5Si_3 interlayer: After 10 cycles of oxidation at 900 °C, the top layer of the dual layered coated TNB-V2 substrate consisted completely of $TiAl_2$ whereas the single layer coated sample only some $TiAl_2$ regions remained within the top layer (Figure 7 and Figure 8). The layer of the dual layered coated TiAl48-2-2 substrate even had some higher amounts of the $TiAl_3$ phase present while the top layer of the single layered TiAl48-2-2 substrate consisted of $TiAl_2$ and TiAl (Figure 7 and Figure 9). Therefore, it can be concluded that Ti_5Si_3 effectively hinders the Al diffusion and counteract the Al depletion. The present results clearly prove that the dual layer coating systems possess a better oxidation resistance. The oxidation behavior could be further increased by a Ti_5Si_3 formation at the grain boundaries of $TiAl_3$ and $TiAl_2$ phases in the Al-Ti top layer as described for Al-Si based coatings [20, 21]. In this case, the Al diffusion towards the substrate is additionally hindered by a longer diffusion path.

4.3. Oxidation behavior during cyclic oxidation test at 900°C

A mass increase below 1 mg/cm^2 after 1000 h is commonly taken as the threshold for oxidation resistance [8]. Both Al-Ti/Ti_5Si_3 dual layered TiAl substrates, TNB-V2 and TiAl48-2-2, as well as the single Al-Ti layer coated TiAl48-2-2 stayed below this threshold indicating a good oxidation resistance (Figure 13). The good resistance based on the high Al content in the top layer and the formation of $TiAl_3$ and $TiAl_2$ phases, whose excellent oxidation behavior has already been described previously in literature [11, 49, 50]. In fact, the parabolic rate constants which were determined in this work are comparable with the literature. Chu et al. showed parabolic rate constants as low as 32×10^{-5} mg^2/(cm^4 h) for a $TiAl_3$ coating deposited by sputtered of Al layer on Ti-50Al (in at.%) alloy with subsequent heat treatment [16]. With a parabolic rate below 10^{-4} mg^2/(cm^4 h), the values published by Smialek [49] were within a comparable range as well. However, the maximum oxidation times reported in the literature were only 100 h which implies that a possible depletion of Al after longer oxidation, as observed in this paper for the single layer coated TNB-V2 sample after 780 1 h cycles, cannot be excluded in published data e.g. by Smialek [49] or Chi et al. [16]. The initial higher mass gain of the dual layered coating systems in comparison to the single layer coatings is most likely a result of the initial formation of the whisker-like metastable θ-Al_2O_3 (Figure 6) [11]. In the β-NiAl Zr system, the oxidation rate of metastable θ-Al_2O_3 is over two magnitudes larger than for the stable α-Al_2O_3 polymorph. [51] It can be assumed that this is also the case for the $TiAl_3$ phase and would therefore explain the higher mass increase of the dual layered samples during the first cycled of oxidation. In comparison, the $TiAl_2$ phase which is present in the Al-Ti top layer without the Ti-Si interlayer develops the stable α-Al_2O_3 polymorph and provides a lower mass gain during the initial oxidation time of 250-300 cycles. During further oxidation, the θ-

Al_2O_3 most likely transforms to α-Al_2O_3 and the steady-state oxidation is established [52]. These results are also in line with the HT-XRD results (Figure 3 and Figure 4) which revealed that during initial heating the single layered coatings depleted in Al and therefore the $TiAl_2$ phase instead of $TiAl_3$ was formed. In contrast, the dual layer coated samples still maintained a higher Al content and therefore $TiAl_3$ was present for 5 to 10 h at 900 °C. After cyclic oxidation at 900 °C for 780 h, the single layer coated TNB-V2 samples showed a rapid linear increase of mass accompanied by the formation of yellow spots on the surface, most likely. The growth of this non-protective oxide occurred when the Al content decreased due to Al_2O_3 formation and inward diffusion of Al from the coating in the substrate. Therefore, the $TiAl_2$ phase transformed to γ-TiAl which possesses a limited oxidation resistance [3]. The obtained results (Figure 5 and Figure 16) show the onset of $TiAl_2$ dissolution in the single layered TNB-V2 samples already after 50 cycles. However, the samples showed a decent oxidation protection for roughly 780 cycles. This allows assuming that an Al-enriched γ-TiAl phase still provides some oxidation resistance, especially when a protective α-Al_2O_3 is already formed. However, when a Ti_5Si_3 interlayer is deposited on the TNB-V2 substrate, followed by an Al-Ti top layer, an excellent oxidation resistance was given for at least 1000 cycles at 900 °C (Figure 15). This is clear evidence that the interlayer helps to increase oxidation resistance. On TiAl48-2-2 substrates, however, the interlayer has a minor positive effect on the oxidation behavior during the first 1000 cycle. This can be seen from the lower mass increase of the dual layer coated sample after 1000 cycles. Nevertheless, it can be assumed that after longer oxidation times a breakaway oxidation of the single layer coated TiAl48-2-2 could occur whereas the dual layer coated sample could still show a parabolic mass increase. Longer cyclic oxidation times could reveal

the beneficial properties of the interlayer on the oxidation behavior of the TiAl48-2-2 sample.

By comparing both single layer coated TiAl substrates, the TiAl48-2-2 alloy did not show any breakaway oxidation during the 1000 hours at 900 °C. Additionally, the Al depletion seemed to occur slower in the Al-Ti top layer on the TiAl48-2-2 in comparison to the TNB-V2 alloy. Both alloys contain Nb, which is known to increase the oxidation resistance of γ-TiAl based alloys [53]. In comparison, Cr can have both a detrimental as well as a positive effect on the oxidation resistance. A detrimental effect was observed in γ-TiAl alloys with low Cr contents of 6 wt.% during oxidation at 700 °C and 900 °C [54, 55] and with Cr contents of 10 at.% at 800 °C and 900 °C [56]. A positive effect on the oxidation resistance was observed with Cr contents of 10 at.% at 1000 °C and 1100 °C due to an enhanced scale adhesion of the TGO as well as the predominant formation of α-Al_2O_3 [56]. This so called “Cr effect” decreases the amount of Al necessary to form α-Al_2O_3 when at least 8-10 at.% of Ti of the TiAl alloy is substituted by Cr [57, 58]. However, it is proposed that the Cr effect occurs during the initial nucleation of the oxides [59]. Since initially no Cr is present in the Al-Ti top layer and the total Cr concentration in the TiAl48-2-2 substrate is just 2 at.%, it is unlikely that the Cr effect occurs in this coating. Therefore, it would be expected that single layer coated the TiAl48-2-2 substrate would have worse oxidation behavior compared to the TNB-V2 alloy and would be more prone to breakaway oxidation. However, this is in contradiction to the results in this work. For that reason the higher Al content in the TiAl48-2-2 alloy (48 at.%), compared with TNB-V2 (45 at.%), seems to be responsible for a lower driving force and therefore slower diffusion. This in turn leads to the absence of breakaway oxidation in the single layer coated TiAl48-2-2 sample. After 1000 cycles of oxidation, the single layer coated TNB-V2 sample also

showed regions of presumably Ti_3Al directly below the interface (Figure 14). These regions could be the starting point for the oxide nodule formation.

5. Conclusions

In this study, magnetron sputtered single layered Al-30Ti (in at.%) coatings were compared with dual layered coating systems consisting of a Al-30Ti top layer and a Ti_5Si_3 interlayer (62Ti-38Si at.%.). Cyclic oxidation tests at 900 °C up to 1000 1-h cycles were conducted in order to observe the behavior of the coating systems during high temperature exposure. The following conclusion can be drawn:

1. The application of the Ti_5Si_3 interlayers has been shown to be an effective way of inhibiting the inward diffusion of Al from the Al-30Ti top coatings into the γ-TiAl alloys – TNB-V2 and TiAl48-2-2. Microstructural investigations revealed that the diffusion of Al in Ti_5Si_3 takes place along the grain boundaries. A faster Al depletion of the Al-Ti coating was observed on the Nb containing TNB-V2 alloy compared with the Cr and Nb containing TiAl48-2-2 one.
2. Dual layer coating systems significantly increase the oxidation resistance of Al-Ti coatings at 900 °C under cyclic oxidation conditions.
3. In the case of the TNB-V2 alloy, the Ti_5Si_3 interlayer completely inhibited the break-away oxidation, which was observed for single-layer Al-Ti coating after 800 1-h cycles at 900 °C.
4. The application of the Ti_5Si_3 interlayer provided a 15 % lower mass increase compared to single-layered Al-Ti coating on TiAl48-2-2 alloy during 1000 1-h cycles of cyclic oxidation.

Acknowledgements

This work was sponsored by the by Deutsche Forschungsgemeinschaft (DFG), Germany under contract Schu1372/6-1 and National Science Centre, Poland under contract UMO-2016/23/G/ST5/04128 within the Beethoven II program - TiAlMET project. The authors thank J. Brien and F. Kreps for the scientific and technical support at the German Aerospace Center as well as R. Anton, Z. Stein and U. Schulz from German Aerospace Center for comments that greatly improved the manuscript.

Data availability statement

The raw and processed data required to reproduce these findings are available on request to peter-philipp.bauer@dlr.de.

6. Literature

[1] M.-R. Yang and S.-K. Wu, "Oxidation resistance improvement of TiAl intermetallics using surface modification," *Bull. Coll. Eng.,* vol. 89, pp. 3-19, 2003 2003.

[2] R. Pflumm, S. Friedle, and M. Schütze, "Oxidation protection of γ-TiAl-based alloys – A review," *Intermetallics,* vol. 56, pp. 1-14, 2015.

[3] M. P. Brady, W. J. Brindley, J. L. Smialek, and I. E. Locci, "The oxidation and protection of gamma titanium aluminides," *JOM,* vol. 48, no. 11, pp. 46-50, 1996/11/01 1996.

[4] H. Clemens and W. Smarsly, "Light-Weight Intermetallic Titanium Aluminides – Status of Research and Development," *Advanced Materials Research,* vol. 278, pp. 551-556, 2011.

[5] R. Swadźba, K. Marugi, and Ł. Pyclik, "STEM investigations of γ-TiAl produced by additive manufacturing after isothermal oxidation," *Corrosion Science,* vol. 169, p. 108617, 2020/06/01/ 2020.

[6] F. Dettenwanger, E. Schumann, M. Ruhle, J. Rakowski, and G. H. Meier, "Microstructural Study of Oxidized γ-TiAl," *Oxidation of Metals,* vol. 50, no. 3, pp. 269-307, 1998/10/01 1998.

[7] S. Becker, A. Rahmel, M. Schorr, and M. Schütze, "Mechanism of isothermal oxidation of the intermetallic TiAl and of TiAl alloys," *Oxidation of Metals,* vol. 38, no. 5-6, pp. 425-464, 1992.

[8] M. Schütze, "The Role of Surface Protection for High-Temperature Performance of TiAl Alloys," *JOM,* Review vol. 69, no. 12, pp. 2602-2609, 2017.

[9] K. L. Luthra, "Stability of protective oxide films on Ti-base alloys," *Oxidation of Metals,* vol. 36, no. 5, pp. 475-490, 1991/12/01 1991.

[10] J. L. Smialek, "Oxidation behaviour of TiAl3 coatings and alloys," *Corrosion Science,* vol. 35, no. 5, pp. 1199-1208, 1993/01/01/ 1993.

[11] V. Gauthier, F. Dettenwanger, M. Schütze, V. Shemet, and W. J. Quadakkers, "Oxidation-Resistant Aluminide Coatings on γ-TiAl," *Oxidation of Metals,* vol. 59, no. 3, pp. 233-255, 2003.

[12] T. C. Munro and B. Gleeson, "The deposition of aluminide and silicide coatings on γ-TiAl using the halide-activated pack cementation method," (in English),

Metallurgical and Materials Transactions A: Physical Metallurgy and Materials Science, Article vol. 27, no. 12, pp. 3761-3772, 1996.

[13] M. S. Chu and S. K. Wu, "The improvement of high temperature oxidation of Ti–50Al by sputtering Al film and subsequent interdiffusion treatment," *Acta Materialia*, vol. 51, no. 11, pp. 3109-3120, 2003/06/27/ 2003.

[14] T. Sasaki, T. Yagi, and T. Watanabe, "Aluminizing of TiAl-Based Alloy Using Thermal Spray Coating," *Materials Science Forum*, vol. 654-656, pp. 1884-1887, 2010.

[15] M. Fröhlich, A. Ebach-Stahl, R. Braun, and C. Leyens, "Oxidation protective coatings for γ-TiAl – recent trends," *Materialwissenschaft und Werkstofftechnik*, vol. 38, no. 9, pp. 667-673, 2007.

[16] M. S. Chu and S. K. Wu, "Oxidation Behavior of Ti-50Al Intermetallics with Thin TiAl3 Film at 1000°C," *Oxidation of Metals*, vol. 63, no. 1-2, pp. 1-13, February 01 2005.

[17] L. Swadzba, A. Maciejny, B. Mendala, G. Moskal, and G. Jarczyk, "Structure and resistance to oxidation of an Al–Si diffusion coating deposited by Arc-PVD on a TiAlCrNb alloy," *Surface and Coatings Technology*, vol. 165, no. 3, pp. 273-280, 2003/02/17/ 2003.

[18] L. Swadzba, G. Moskal, M. Hetmanczyk, B. Mendala, and G. Jarczyk, "Long-term cyclic oxidation of Al–Si diffusion coatings deposited by Arc-PVD on TiAlCrNb alloy," *Surface and Coatings Technology*, vol. 184, no. 1, pp. 93-101, 2004.

[19] J. Wang, L. Kong, T. Li, and T. Xiong, "Microstructure Evolution of Cold-Sprayed Al-Si Alloy Coatings on γ-TiAl During Heat Treatment," *Journal of Thermal Spray Technology*, vol. 24, no. 6, pp. 1071-1080, 2015/08/01 2015.

[20] J. Wang, L. Kong, J. Wu, T. Li, and T. Xiong, "Microstructure evolution and oxidation resistance of silicon-aluminizing coating on γ-TiAl alloy," *Applied Surface Science*, vol. 356, pp. 827-836, 2015/11/30/ 2015.

[21] P.-P. Bauer, N. Laska, and R. Swadźba, "Increasing the oxidation resistance of γ-TiAl by applying a magnetron sputtered aluminum and silicon based coating," *Intermetallics*, vol. 133, p. 107177, 2021/06/01/ 2021.

[22] K. Bobzin, T. Brögelmann, C. Kalscheuer, and T. Liang, "High temperature oxidation protection of γ-titanium aluminide using (Cr,Al)ON coatings deposited by high-speed physical vapor deposition," *Surface and Coatings Technology*, vol. 332, pp. 2-11, 2017.

[23] K. Bobzin, T. Brögelmann, C. Kalscheuer, and T. Liang, "Al-Si and Al-Si-Y coatings deposited by HS-PVD for the oxidation protection of γ-TiAl," *Surface and Coatings Technology*, vol. 350, pp. 587-595, 2018/09/25/ 2018.

[24] K. Bobzin, T. Brögelmann, C. Kalscheuer, T. Liang, C. H., and K. H., "Thermal cyclic oxidation behavior of γ-TiAl with in situ post-annealed Al-Si-Y coating," vol. 37, no. 4, p. 041401, 2019.

[25] M. Goral, G. Moskal, L. Swadźba, and M. Hetmańczyk, "The Influence of Silicon Amount on Structure of Si Modified Aluminide Coating Deposited on Ti46Al7Nb Alloy by Slurry Method," *Key Engineering Materials*, vol. 465, pp. 251-254, 2011.

[26] M. Goral, L. Swadzba, G. Moskal, M. Hetmanczyk, and T. Tetsui, "Si-modified aluminide coatings deposited on Ti46Al7Nb alloy by slurry method," *Intermetallics*, vol. 17, no. 11, pp. 965-967, 2009.

[27] Z. D. Xiang, S. R. Rose, J. S. Burnell-Gray, and P. K. Datta, "Co-deposition of aluminide and silicide coatings on γ-TiAl by pack cementation process," *Journal of Materials Science,* Article vol. 38, no. 1, pp. 19-28, 2003.

[28] Z. D. Xiang, S. R. Rose, and P. K. Datta, "Codeposition of Al and Si to form oxidation-resistant coatings on γ-TiAl by the pack cementation process," *Materials Chemistry and Physics,* vol. 80, no. 2, pp. 482-489, 2003.

[29] H.-P. Xiong *et al.*, "Liquid-phase aluminizing and siliconizing at the surface of a Ti60 alloy and improvement in oxidation resistance," *Materials Science and Engineering: A,* vol. 433, no. 1, pp. 108-113, 2006/10/15/ 2006.

[30] H. P. Xiong, M. Wei, Y. H. Xie, Y. Y. Cheng, and X. H. Li, "Formation of silicide coatings on the surface of a TiAl-based alloy and improvement in oxidation resistance," (in English), *Materials Science and Engineering a-Structural Materials Properties Microstructure and Processing,* vol. 391, no. 1-2, pp. 10-18, Jan 25 2005.

[31] R. Swadźba *et al.*, "Characterization of Si-aluminide coating and oxide scale microstructure formed on γ-TiAl alloy during long-term oxidation at 950 °C," *Intermetallics,* vol. 87, pp. 81-89, 2017.

[32] A. Knaislová, P. Novák, M. Cabibbo, L. Jaworska, and D. Vojtěch, "Development of TiAl–Si Alloys—A Review," vol. 14, no. 4, p. 1030, 2021.

[33] T. B. Massalski, H. Okamoto, and A. S. M. International, *Binary alloy phase diagrams*. Materials Park, Ohio: ASM International, 1990.

[34] X. Sun, J. S. Reid, E. Kolawa, M.-A. Nicolet, and R. P. Ruiz, "Reactively sputtered Ti-Si-N films. II. Diffusion barriers for Al and Cu metallizations on Si," vol. 81, no. 2, pp. 664-671, 1997.

[35] V. K. Tolpygo and D. R. Clarke, "Microstructural study of the theta-alpha transformation in alumina scales formed on nickel-aluminides," *Materials at High Temperatures,* vol. 17, no. 1, pp. 59-70, 2000/01/01 2000.

[36] B. Pieraggi, "Calculations of parabolic reaction rate constants," *Oxidation of Metals,* vol. 27, no. 3, pp. 177-185, 1987/04/01 1987.

[37] C. Herzig, T. Przeorski, M. Friesel, F. Hisker, and S. Divinski, "Tracer solute diffusion of Nb, Zr, Cr, Fe, and Ni in γ-TiAl: effect of preferential site occupation," *Intermetallics,* vol. 9, no. 6, pp. 461-472, 2001/06/01/ 2001.

[38] J. A. Thornton, "The microstructure of sputter-deposited coatings," *Journal of Vacuum Science & Technology A: Vacuum, Surfaces, and Films,* vol. 4, no. 6, pp. 3059-3065, 1986.

[39] J. C. Schuster and M. Palm, "Reassessment of the binary Aluminum-Titanium phase diagram," *Journal of Phase Equilibria and Diffusion,* vol. 27, no. 3, pp. 255-277, 2006/06/01 2006.

[40] N. Laska, S. Friedle, R. Braun, and M. Schütze, "Lifetime of 7YSZ thermal barrier coatings deposited on fluorine-treated γ-TiAl-based TNM-B1 alloy," vol. 67, no. 11, pp. 1185-1194, 2016.

[41] J. Braun and M. Ellner, "Phase equilibria investigations on the aluminum-rich part of the binary system Ti-Al," *Metallurgical and Materials Transactions A,* vol. 32, no. 5, pp. 1037-1047, 2001/05/01 2001.

[42] C. R. de Farias Azevedo and H. M. Flower, "Microstructure and phase relationships in Ti–Al–Si system," *Materials Science and Technology,* vol. 15, no. 8, pp. 869-877, 1999/08/01 1999.

[43] M. Zha, H. Y. Wang, S. T. Li, S. L. Li, Q. L. Guan, and Q. C. Jiang, "Influence of Al addition on the products of self-propagating high-temperature synthesis of

Al–Ti–Si system," *Materials Chemistry and Physics,* vol. 114, no. 2, pp. 709-715, 2009/04/15/ 2009.
[44] M. Bulanova, L. Tretyachenko, M. Golovkova, and K. Meleshevich, "Phase equilibria in the α-Ti-Al-Si region of the Ti-Si-Al system," *Journal of Phase Equilibria and Diffusion,* vol. 25, no. 3, pp. 209-229, 2004/08/01 2004.
[45] J. O. Andersson, T. Helander, L. Höglund, P. Shi, and B. Sundman, "Thermo-Calc & DICTRA, computational tools for materials science," *Calphad,* vol. 26, no. 2, pp. 273-312, 2002/06/01/ 2002.
[46] J. Wang, Y. Liu, Y. Liu, C. Wu, and X. Su, "The Isothermal Section of the Al-Si-Ti Ternary System at 550 °C," *Journal of Phase Equilibria and Diffusion,* vol. 40, no. 6, pp. 810-819, 2019/12/01 2019.
[47] H. Mehrer and S. V. Divinski, "Diffusion in Metallic Elements and Intermetallics," *Defect and Diffusion Forum,* vol. 289-292, pp. 15-38, 2009.
[48] L. G. Harrison, "Influence of dislocations on diffusion kinetics in solids with particular reference to the alkali halides," (in en), *Transactions of the Faraday Society,* vol. 57, p. 1191, 1961 1961.
[49] J. L. Smialek, "Oxidation behaviour of $TiAl_3$ coatings and alloys," *Corrosion Science,* vol. 35, no. 5–8, pp. 1199-1208, 1993.
[50] Y. Umakoshi, M. Yamaguchi, T. Sakagami, and T. Yamane, "Oxidation resistance of intermetallic compounds Al3Ti and TiAl," *Journal of Materials Science,* vol. 24, no. 5, pp. 1599-1603, 1989/05/01 1989.
[51] G. C. Rybicki and J. L. Smialek, "Effect of the θ-α-Al2O3 transformation on the oxidation behavior of β-NiAl + Zr," *Oxidation of Metals,* vol. 31, no. 3, pp. 275-304, 1989/04/01 1989.
[52] R. Swadźba, L. Swadźba, B. Mendala, P.-P. Bauer, N. Laska, and U. Schulz, "Microstructure and cyclic oxidation resistance of Si-aluminide coatings on γ-TiAl at 850 °C," *Surface and Coatings Technology,* vol. 403, p. 126361, 2020/12/15/ 2020.
[53] H. Nickel, N. Zheng, A. Elschner, and W. J. Quadakkers, "The oxidation behaviour of niobium containing γ-TiAl based intermetallics in air and argon/oxygen," *Microchimica Acta,* vol. 119, no. 1, pp. 23-39, 1995/03/01 1995.
[54] B. G. Kim, G. M. Kim, and C. J. Kim, "Oxidation behavior of TiAl-X (X = Cr, V, Si, Mo or Nb) intermetallics at elevated temperature," *Scripta Metallurgica et Materialia,* vol. 33, no. 7, pp. 1117-1125, 1995/10/01/ 1995.
[55] Y. Shida and H. Anada, "The effect of various ternary additives on the oxidation behavior of TiAl in high-temperature air," *Oxidation of Metals,* vol. 45, no. 1, pp. 197-219, 1996/02/01 1996.
[56] F. Wang, Z. Tang, and W. Wu, "Effect of chromium on the oxidation resistance of TiAl intermetallics," *Oxidation of Metals,* vol. 48, no. 5, pp. 381-390, 1997/12/01 1997.
[57] M. P. Brady, J. L. Smialek, D. L. Humphrey, and J. Smith, "The role of Cr in promoting protective alumina scale formation by γ-based Ti・Al・Cr alloys— II. Oxidation behavior in air," *Acta Materialia,* vol. 45, no. 6, pp. 2371-2382, 1997/06/01/ 1997.
[58] M. P. Brady, J. L. Smialek, J. Smith, and D. L. Humphrey, "The role of Cr in promoting protective alumina scale formation by γ-based Ti・Al・Cr alloys—I. Compatibility with alumina and oxidation behavior in oxygen," *Acta Materialia,* vol. 45, no. 6, pp. 2357-2369, 1997/06/01/ 1997.
[59] G. S. Fox-Rabinovich, G. C. Weatherly, D. S. Wilkinson, A. I. Kovalev, and D. L. Wainstein, "The role of chromium in protective alumina scale formation during

the oxidation of ternary TiAlCr alloys in air," *Intermetallics,* vol. 12, no. 2, pp. 165-180, 2004/02/01/ 2004.